

# Plasma-Balls in Large $N$ Gauge Theories and Localized Black Holes

Ofer Aharony<sup>a,1</sup>, Shiraz Minwalla<sup>b,c,2</sup> and Toby Wiseman<sup>c,3</sup>

<sup>a</sup>*Department of Particle Physics, Weizmann Institute of Science, Rehovot 76100, Israel*

<sup>b</sup>*Department of Theoretical Physics, Tata Institute of Fundamental Research,  
Homi Bhabha Rd, Mumbai 400005, India*

<sup>c</sup>*Jefferson Physical Laboratory, Harvard University, Cambridge, MA 02138, USA*

We argue for the existence of plasma-balls – meta-stable, nearly homogeneous lumps of gluon plasma at just above the deconfinement energy density – in a class of large  $N$  confining gauge theories that undergo first order deconfinement transitions. Plasma-balls decay over a time scale of order  $N^2$  by thermally radiating hadrons at the deconfinement temperature. In gauge theories that have a dual description that is well approximated by a theory of gravity in a warped geometry, we propose that plasma-balls map to a family of classically stable finite energy black holes localized in the IR. We present a conjecture for the qualitative nature of large mass black holes in such backgrounds, and numerically construct these black holes in a particular class of warped geometries. These black holes have novel properties; in particular their temperature approaches a nonzero constant value at large mass. Black holes dual to plasma-balls shrink as they decay by Hawking radiation; towards the end of this process they resemble ten dimensional Schwarzschild black holes, which we propose are dual to small plasma-balls. Our work may find practical applications in the study of the physics of localized black holes from a dual viewpoint.

July 2005

---

<sup>1</sup> E-mail : Ofer.Aharony@weizmann.ac.il.

<sup>2</sup> E-mail : minwalla@theory.tifr.res.in.

<sup>3</sup> E-mail : twiseman@fas.harvard.edu.

## Contents

1. Introduction and Summary . . . . .	2
1.1. Meta-stable Bubbles of Plasma in Confining Large $N$ Gauge Theories . . . . .	2
1.2. Black Holes in the IR . . . . .	3
1.3. Plasma-Balls as Black Holes . . . . .	5
2. The Plasma-ball as a Stable Lump of Plasma Fluid . . . . .	7
3. Hadronization of Plasma-Balls at Large $N$ . . . . .	10
3.1. Counting Powers of $N$ . . . . .	11
3.2. $k=0$ : Gluon Mean Free Time . . . . .	12
3.3. $k=1$ : Glueball Production Rate . . . . .	12
3.4. $k=2$ : Friction . . . . .	13
4. Localized Black Holes in Warped Backgrounds . . . . .	13
5. Localized Black Holes as Plasma-balls . . . . .	16
6. Plasma-Ball Dynamics from Black Holes . . . . .	18
6.1. Plasma-Ball Hadronization as Hawking Radiation . . . . .	18
6.2. Plasma-Ball Production in Hadron-Hadron Collisions . . . . .	18
7. Black Hole Physics from Gluon Plasmas . . . . .	20
7.1. The Fate of Small Schwarzschild Black Holes . . . . .	21
7.2. Information Conservation in Hawking Radiation . . . . .	21
7.3. How Black is a Black Hole ? . . . . .	22
8. Numerical Solutions for Domain Walls in some Specific Backgrounds . . . . .	23
8.1. Scherk-Schwarz Compactifications of Anti-De Sitter Space . . . . .	23
8.2. The Domain Wall: Asymptotic Behaviors . . . . .	25
Appendix A. Thermodynamics of Large $N$ Gauge Theories . . . . .	34
A.1. Local Stability of Homogeneous Configurations . . . . .	34
A.2. Density of States in Confining Gauge Theories . . . . .	35
A.3. Phase Separation in Confining Large $N$ gauge theories . . . . .	37
Appendix B. Properties of Plasma Dynamics . . . . .	38
B.1. The Surface Tension of the Plasma-Ball . . . . .	38
B.2. Dynamical Evolution of Lumps of Plasma . . . . .	39
B.3. Small Plasma-Balls . . . . .	40
B.4. Plasma Lumps in Theories with Second Order Deconfinement Transitions . . . . .	40
B.5. Plasma-Balls in the Real World ? . . . . .	40
Appendix C. Counting Powers of $N$ at Lowest Order in Perturbation Theory . . . . .	41
C.1. $k = 0$ : Mean Free Path . . . . .	41
C.2. $k = 1$ : Rate of Glueball Production . . . . .	42
Appendix D. The Final Decay of Small Plasma-Balls . . . . .	43
Appendix E. The Boundary Stress Tensor for Compactifications of $AdS_{d+2}$ . . . . .	44
Appendix F. Numerical Construction of the Domain Wall Solution . . . . .	44
F.1. Equations and Constraints . . . . .	44
F.2. The IR Boundary Conditions . . . . .	46
F.3. The UV Boundary Conditions . . . . .	47
F.4. Solving the Constraint System . . . . .	51
F.5. Summary . . . . .	52

Appendix G. Numerical Details . . . . .	52
References . . . . .	56

## 1. Introduction and Summary

In this paper we study the spectrum of localized excitations in confining large  $N$  gauge theories with energies of order  $N^2$ , the spectrum of static black holes in warped geometries with an effective infrared wall, and the connection between these two spectra, using generalizations of the AdS/CFT correspondence. In the rest of this section we will first introduce each of these questions and then explain the relationship between them. Readers who are only interested in gauge theory aspects may read sections 1.1, 2 and 3 and appendices A, B, C, which are independent of the rest of the paper.

### 1.1. Meta-stable Bubbles of Plasma in Confining Large $N$ Gauge Theories

It has long been believed [1] that confining large  $N$   $SU(N)$  gauge theories are dual to weakly coupled string theories with a string coupling  $g_s \propto 1/N$ . The string duals possess an exponential tower of long lived excitations (perturbative string states) which are identified with glueballs. However, at least some perturbative string theories also possess other long lived excitations – black holes – at energies of order  $1/g_s^2$ . In this paper we argue that such configurations have analogues in a class of confining large  $N$  gauge theories (for earlier related works see [2,3]).

Consider a confining large  $N$  gauge theory, with mass gap  $\Lambda_{gap}$ , whose thermal deconfinement phase transition is of first order (e.g. pure Yang Mills theory at large  $N$  [4,5]). In this paper we argue that, provided the theory in question obeys one additional condition (see section 2), it hosts long lived excitations at all masses  $m \gg N^2 \Lambda_{gap}$ . We call these meta-stable configurations plasma-balls. Plasma-balls are spherical, approximately homogeneous lumps of deconfined plasma fluid, whose energy density is just above the critical density (which is the energy density at the deconfinement phase transition temperature  $T_d$ ; this energy density is of order  $N^2$  in the large  $N$  limit). These lumps are static because the pressure of the plasma in such theories vanishes at the critical energy density.

Of course a plasma-ball is not completely stable; eventually it decays into a gas of hadrons. In section 3 we study the  $N$  dependence of the processes that contribute to this decay, and conclude that the hadronization of the plasma-ball is very slow in the large

$N$  limit. Even though the density of the plasma-ball is of order  $N^2$ , and the number of gluon-gluon interactions per unit time within the plasma-ball is of order  $N^2$ , glueballs are produced from these collisions at a rate that is independent of  $N$ . Intuitively, only  $1/N^2$  of the gluon-gluon collisions – collisions between a gluon and its color anti-partner – can form a singlet state that can escape from the plasma.

Large  $N$  counting is insufficient to determine the precise rate of radiation of glueballs as a function of (for instance) their mass; however the thermal nature of the plasma-ball suggests that these rates are controlled by the Boltzmann factor at the temperature of the plasma-ball. We conjecture that this is indeed the case. In a class of examples described below, the dual gravitational description of plasma-balls confirms this conjecture.

We have already explained that the rate of radiation of any given glueball from the surface of a plasma-ball is independent of  $N$ . Using the conjecture of the previous paragraph and the expectation that the density of glueball species at high energies is proportional to  $\exp(E/T_H)$  where  $T_H$  is the Hagedorn temperature, the rate of loss of energy integrated over all glueball species is proportional to  $\int \exp\left(\left(\frac{1}{T_H} - \frac{1}{T_d}\right) E\right) dE$ . As the deconfinement temperature is strictly smaller than the Hagedorn temperature in theories that undergo first order deconfinement transitions [6,7], this is a finite number of order  $N^0$ . As a consequence, the lifetime of a plasma-ball of radius  $R$  ( $R \gg 1/\Lambda_{gap}$ ) is of order  $N^2 R$ .

Note that QCD at zero chemical potential (for baryon number) does not undergo a first order phase transition as a function of temperature. Thus, we do not expect plasma-ball-like meta-stable configurations to be created in experiments like RHIC<sup>4</sup>. See appendix B.5 for further discussion.

### 1.2. Black Holes in the IR

We start this subsection by characterizing the class of warped geometries whose black holes we study. Consider any solution to Einstein's equations coupled to appropriate matter fields, whose metric can be put in the form

$$ds^2 = \alpha' L^2 (W^2(u) dx_\mu^2 + ds_{int}^2), \quad (1.1)$$

---

<sup>4</sup> Dynamical plasma configurations which are dual to dynamical black holes could perhaps be related to RHIC, as suggested by Nastase and collaborators [3]. In this context note that the decay products of the RHIC fireball have a distribution which is close to thermal, at approximately the deconfinement crossover temperature.

where  $\mu = 0, 1, 2, \dots, p$ ,  $\alpha' L^2$  is a constant with units of length squared, and  $ds_{int}^2$  is the metric on an internal manifold, one of whose coordinates is  $u$ , and whose constant  $u$  slices are compact. The variable  $u$  in (1.1) has the range  $u_0 < u < \infty$  and the function  $W(u)$  increases monotonically from a positive nonzero value at  $u_0$  to infinity at  $u = \infty$ . We assume that (1.1) is smooth and without boundaries everywhere, including at the IR wall  $u = u_0$ <sup>5</sup>. We further assume that the space in question has well defined thermodynamics (in particular it admits the definition of an ADM mass), and that the spectrum of fluctuations about (1.1) is gapped. Examples include the confining backgrounds constructed in [8,9,10].<sup>6</sup>

We are interested in backgrounds (1.1) which have an additional property; they host black brane solutions of finite energy density<sup>7</sup> at all energy densities larger than a critical value  $\rho_e$ . Moreover, these branes are required to be stable (and have positive specific heat) above  $\rho_s > \rho_e$ , and to have negative free energy density above  $\rho_c > \rho_s$ . Let  $T_d$  denote the temperature of the black brane of energy density  $\rho_c$ . Assuming that there are no other phases of the theory, it follows that the thermodynamics in this background is dominated by a graviton gas about (1.1) for  $T < T_d$ , and by the black brane for  $T > T_d$ ; the system undergoes a first order phase transition at  $T = T_d$ .

In this paper we conjecture that spaces that obey all these properties possess a one parameter set of spherically symmetric (in  $p$  dimensions) black hole solutions<sup>8</sup> labeled by their mass, and that, in the large mass limit, these black holes have the following properties:

1. Their volume in  $p$  dimensions is proportional to their mass, i.e. the radius of the black hole in  $p$  dimensions scales with mass like  $(m/\rho_c)^{1/p}$ .
2. In the interior (meaning away from the edges in the  $\mathbb{R}^p$  spatial directions, not the black hole interior behind the horizon) these black hole solutions approximate the black brane at energy density  $\rho_c$ .

---

<sup>5</sup> This is possible because a  $k$ -cycle of the internal manifold shrinks to zero size at  $u = u_0$ , so that, locally,  $u - u_0$  may simply be thought of as the radial coordinate of an  $\mathbb{R}^{k+1}$  component of the geometry.

<sup>6</sup> The background of [9] actually does not have a mass gap [11], but we expect that our analysis should still apply to it.

<sup>7</sup> More precisely, there exist smooth gravitational solutions with horizons, asymptoting to (1.1), which preserve translational invariance in  $\mathbb{R}^p$  and have a finite energy density above that of the background (1.1).

<sup>8</sup> Black holes in this context were first discussed in [2].

3. In the vicinity of their edge the solutions reduce to a domain wall in the  $\mathbb{R}^p$  directions, that interpolates between the black brane at the critical energy density  $\rho_c$  at one end, and the background (1.1) at the other end.

We emphasize that the black holes described in the previous paragraph have thermodynamical properties that are qualitatively different from black holes in flat space; in particular their temperature tends to a finite value  $T_d$  in the limit of infinite mass.

In section 4 we use intuitive arguments to motivate the conjecture described above. In addition, as concrete evidence for our conjecture, in section 8 we present a numerical construction of the domain wall about a particularly simple background of the form (1.1). The background [8] we study is a solution to Einstein's equations with a negative cosmological constant but no other matter fields, and asymptotes to a Scherk-Schwarz circle compactification of Lorentzian  $AdS_{d+2}$ , or (at finite temperature in Euclidean space) to a torus compactification of Euclidean  $AdS_{d+2}$ . An infinite series of translationally invariant (in  $d - 1$  dimensions) solutions with these asymptotics is known. The topology of each of these solutions is  $\mathbb{R}^d$  times the solid torus; the distinct solutions are labeled by which cycle of the boundary torus is 'filled in' in the solution. When the boundary torus is rectangular, the thermodynamics is dominated by the solution that fills the smaller of the (1, 0) and (0, 1) cycles. A phase transition between these two solutions occurs when the boundary torus is a square. In section 8 we give an overview of the numerical construction of the domain wall solution that interpolates between these two solutions at the phase transition temperature, and compute the (positive) surface tension of this domain wall. More details of our construction may be found in appendices F and G, and an example of the program used to generate the solutions may be downloaded from <http://schwinger.harvard.edu/~wiseman/IRblackholes/> .

### 1.3. Plasma-Balls as Black Holes

Dual string descriptions of large  $N$   $SU(N)$  gauge theories are expected to exist on general grounds from 't Hooft's analysis of the large  $N$  limit [1]. The dual string coupling is always proportional to  $1/N$ , so the interactions between strings are small in the large  $N$  limit. Unfortunately the string duals to most familiar confining gauge theories (such as pure  $SU(N)$  Yang-Mills theory) have yet to be discovered; furthermore, the relevant dual dynamics may be argued to be controlled by a strongly coupled worldsheet theory that does not admit a truncation to the lowest (gravitational) sector. In several examples [8,12,9,10], however, it turns out to be possible to modify standard confining gauge theories

by coupling them to a judiciously chosen set of additional degrees of freedom. The energy scale of ‘new physics’ is a free parameter, which is most conveniently labeled by the value of the ‘t Hooft coupling  $\lambda \equiv g_{YM}^2 N$  at the scale of new physics. In the limit  $\lambda \rightarrow 0$  the scale of new physics is much higher than the mass gap, and, at low energies compared to the scale of the new physics, we recover the (strongly coupled) dynamics of the original confining theory. In the opposite limit of large  $\lambda$ , the new degrees of freedom give large anomalous dimensions to all operators that create glueballs dual to string oscillators. As a consequence such glueballs have masses that are parametrically higher than the graviton, and the low energy dual dynamics reduces to a theory of gravity (usually ten dimensional supergravity) in a warped background. In specific examples [8,12,9,10] this gravitational dual may explicitly be identified using a generalization of the AdS/CFT correspondence. In each case the resulting gravitational theory lives in a warped geometry of the form (1.1) (for a  $p + 1$ -dimensional confining gauge theory) that obeys all the conditions of the previous subsection, and so, according to our conjecture, hosts localized black holes. Since the ‘black brane nucleation’ phase transitions in these geometries may be identified with deconfinement transitions in the dual field theory [8], it follows that these localized black holes are dual to plasma-balls (see [2,13,3] for related remarks).

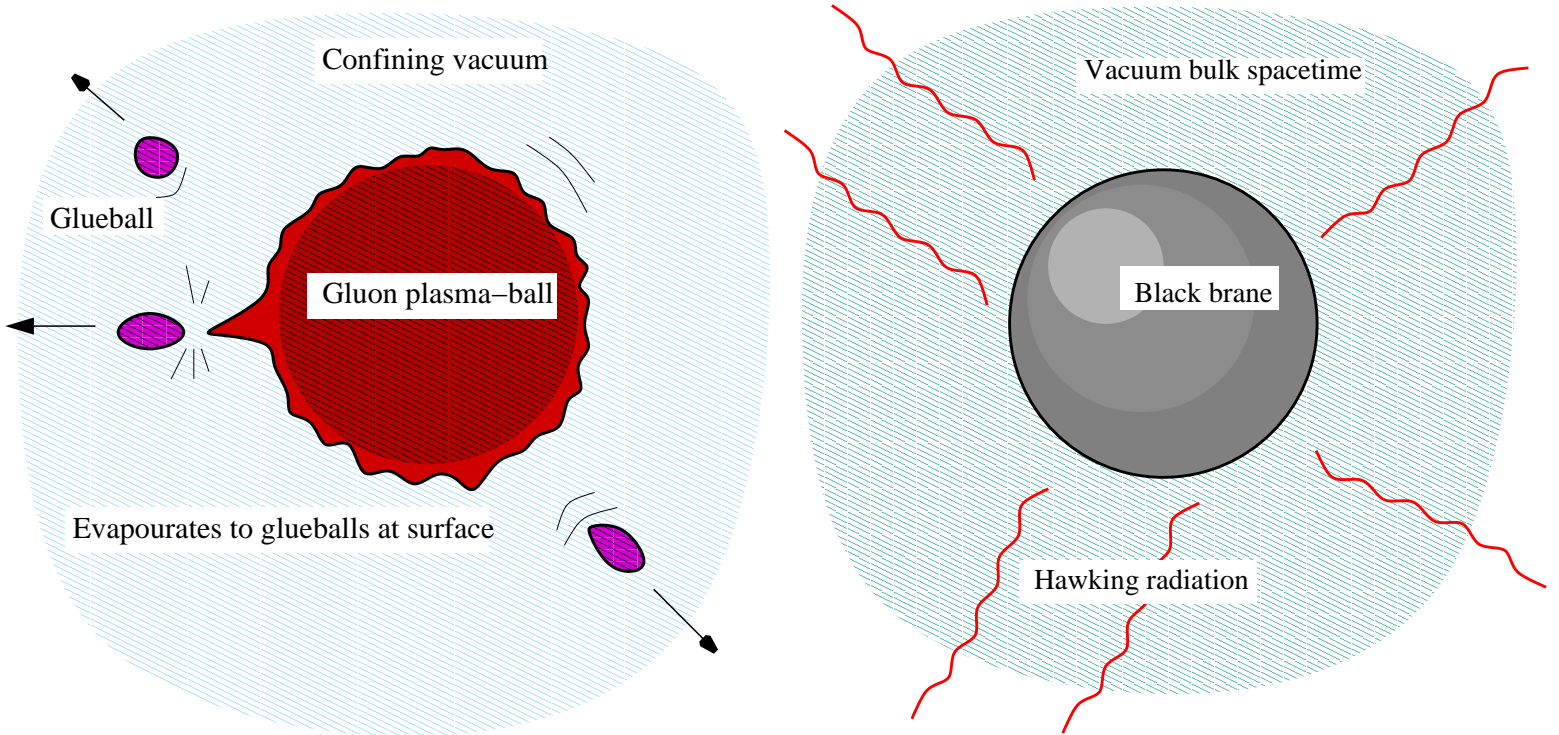


**Figure 1:** The plasma-ball and its decay via hadronization (left), and the localized black hole and its decay via Hawking radiation (right).

The decay of the plasma-ball by hadronization maps to the decay of its dual black hole by Hawking radiation. It follows that, at least at large  $\lambda$ , the decay of plasma-balls is a thermal process at the temperature  $T_d$ , in agreement with the guess described in §1.1.

Even in warped backgrounds, high energy graviton-graviton collisions are likely to be dominated by black hole formation [2,3]. It follows that, in confining theories at large  $\lambda$ , high energy hadron-hadron collisions are dominated by plasma-ball production. Of course, plasma-ball formation does not dominate high energy glueball-glueball collisions at small  $\lambda$ . In Section 6 we trace these different behaviors to qualitative differences in the hadron parton distribution functions at small and large  $\lambda$  [14].

The duality with plasma-balls could yield interesting lessons for black hole physics. As we have explained above, at large  $\lambda$  the production of a plasma-ball in high energy hadron-hadron collisions, and its subsequent decay by hadronization, is dual to the production of a black hole in high energy graviton-graviton scattering, and its subsequent decay by Hawking radiation. As the first of these processes is manifestly unitary, its dual must be as well. It is possible that this connection could be pursued further to draw more detailed lessons about the nature of the Hawking radiation process.

As a second application, we argue in section 7 that one of the most striking features of black hole physics – the universally absorptive nature of black holes – is crucially tied to a feature of the hadronic parton distribution function at large  $\lambda$  that is absent at small  $\lambda$ . It follows that while black hole like configurations continue to exist in at least some warped geometries with curvatures of order the string scale (those that are dual to gauge theories at small  $\lambda$ ), they have qualitatively different dynamics from their large  $\lambda$  cousins. In particular they are no longer black.

## 2. The Plasma-ball as a Stable Lump of Plasma Fluid

In this elementary sub-section we will argue for the existence of a meta-stable localized lump of plasma fluid (in the deconfined phase) – a plasma-ball – in certain large  $N$  theories that undergo first order phase transitions. More details may be found in appendix A.

Consider an isolated spherical ball of static plasma fluid of radius  $R \gg 1/\Lambda_{gap}$  in  $p$  spatial dimensions. In equilibrium its effective temperature  $T$  and the pressure  $P$  are



both uniform in the bulk of the ball<sup>9</sup>. In order for the ball to be static, the pressure of the plasma in the ball must precisely balance the tension of the domain wall separating the two phases (the “surface tension” of the plasma fluid; see appendix B.1 for a precise definition). Denoting this tension by  $\Sigma$ , the forces balance when

$$\omega_{p-2}R^{p-2}\Sigma = \frac{\omega_{p-2}}{p-1}R^{p-1}P \quad \implies \quad P = \frac{(p-1)\Sigma}{R}, \quad (2.1)$$

where  $\omega_{p-2}$  is the surface area of the unit  $(p-2)$ -sphere, and  $\omega_{p-2}/(p-1)$  is the volume of the unit  $(p-1)$ -ball. Since the bubble is in the deconfined phase, its pressure and surface tension are both of order  $N^2$ <sup>10</sup>, and are functions of the plasma-ball temperature. According to (2.1), static plasma-balls exist at asymptotically large  $R$  if and only if the pressure of the deconfined phase vanishes at a finite temperature.

While the precise functional form of  $P(T)$  (the pressure of the deconfined phase as a function of temperature) depends on details, this function is constrained by thermodynamic considerations. First, a simple thermodynamical identity (see appendix A) ensures that the pressure increases monotonically with temperature, provided that the specific heat of the deconfined phase is positive. Second, as pressure is continuous across a phase transition, the pressure of the deconfined phase is  $\mathcal{O}(1)$  (rather than the generic  $\mathcal{O}(N^2)$ ) at the deconfinement temperature  $T_d$ . Provided that the phase transition is of first order (an assumption we will make in most of the rest of this paper) the specific heat, and so  $dP/dT$ , are positive and of order  $N^2$  at  $T = T_d$  (see appendix A)<sup>11</sup>. It follows that the pressure of the deconfined plasma vanishes at  $T = T_d - \mathcal{O}(1/N^2)$ . We conclude that uniform, asymptotically large lumps of fluid plasma are static at the deconfinement temperature in large  $N$  gauge theories that undergo first order phase transitions. Provided that  $\Sigma$  is positive, large but finite static spherical lumps of plasma fluid exist at a temperature

---

<sup>9</sup> In this section we ignore energy loss by ‘radiation’ from the surface of the plasma-ball. In the next section we will argue that this approximation is justified in the large  $N$  limit. The energy loss by radiation to the bulk is  $\mathcal{O}(1)$ ; as the energy density within the plasma ball is  $\mathcal{O}(N^2)$ , the temperature gradients induced by surface radiation are negligible in the large  $N$  limit.

<sup>10</sup> As we review in appendix A, the pressure is simply minus the free energy density of the bubble. The fact that the surface tension should scale as  $N^2$  is predicted from general arguments, since planar diagrams should contribute to it, but it has not yet been directly verified by lattice computations [4].

<sup>11</sup> More precisely this is true of the limit of the specific heat, as  $T$  approaches  $T_d$  from above. This limit determines the speed of sound of the deconfined plasma fluid within the plasma-ball.

slightly above the deconfinement temperature, and have an energy density slightly above the critical energy density.

These static lumps are also hydrodynamically stable <sup>12</sup>, provided that the effective surface tension is positive. As we have assumed the deconfinement transition to be of first order, the deconfined phase continues to exist (as a meta-stable phase) at temperatures below  $T_d$ . As we have explained in the previous paragraph, the pressure of the deconfined phase is positive for  $T > T_d$  and negative for  $T < T_d$ ; it follows that plasma-balls are stable against homogeneous expansion or contraction. Local stability of the plasma fluid against density fluctuations in the bulk of the ball follows from the positivity of the speed of sound at the phase transition temperature (see appendix A). Linearized long wavelength fluctuations of the surface also obey a wave equation; the squared speed of sound of these surface waves is proportional to the effective surface tension; as a consequence the plasma-ball is stable to fluctuations of the boundary provided that this surface tension is positive and approaches a finite value at the deconfinement temperature.

Note that according to (2.1) the pressure (hence temperature) of a plasma-ball with positive surface tension is a decreasing function of its radius (hence mass), so plasma-balls have negative specific heat <sup>13</sup>. Of course, plasma-balls are not completely stable; they eventually hadronize. In the next section we discuss this hadronization process. Additional discussions of various aspects of plasma dynamics may be found in appendix B.

In this section we have, so far, discussed plasma-balls that carry no conserved charges besides their energy, and we will focus on such configurations in the remainder of the paper. However the hydrodynamical construction of stationary lumps of plasma generalizes in a straightforward manner upon adding other conserved charges. As a simple example consider a radially symmetric lump of plasma rotating with angular velocity  $\omega$  (about the origin) in  $p = 2$  spatial dimensions. Force balance yields the equation

$$\frac{dP}{dr} = \rho(r)\omega^2 r, \tag{2.2}$$

---

<sup>12</sup> They resemble the bubbles of the deconfined phase which appear when the energy density of the system is gradually raised through the first order phase transition, except for the fact that they live in the vacuum.

<sup>13</sup> Note that the (negative) specific heat of the plasma-ball as an object is distinct from the (positive) specific heat per unit volume of the deconfined phase of which the plasma-ball is composed.

where  $P(r)$  and  $\rho(r)$  are the pressure and density at radial distance  $r$ , and we have used the non-relativistic approximation appropriate for small rotational velocities. Substituting  $\rho$  as a function of  $P$  using the equation of state, we find

$$\int_{P(r)}^{\Sigma/R} \frac{dP}{\rho(P)} = \frac{\omega^2}{2}(R^2 - r^2). \quad (2.3)$$

This may be regarded as an equation for  $P(r)$ , and potentially it can have two qualitatively distinct classes of solutions. In solutions of the first class the variable  $r$  has the range  $(0, R)$ . Such a solution may be thought of as a rotating plasma-ball. In the second class of solutions  $r$  has the range  $(R_1, R)$ , and (2.3) is to be solved subject to the boundary condition  $P(R_1) = -\Sigma/R_1$  (we assume  $R, R_1 \gg 1/\Lambda_{gap}$ ). Such a solution is best thought of as a rotating plasma-ring, filling an annulus in the plane.

### 3. Hadronization of Plasma-Balls at Large $N$

In this section we will compute the  $N$  dependence of the rate at which a plasma-ball hadronizes (decays into glueballs). We model the plasma-ball as a gas of initially thermally distributed uncorrelated gluons, whose collisions sometimes produce glueballs. We then determine the  $N$  dependence of all Feynman graphs (with arbitrary numbers of interaction vertices) that contribute to glueball production. We find that the rate at which any particular glueball is produced is independent of  $N$ .

Of course, the gluonic constituents of a plasma-ball are not really uncorrelated; however all correlations may be switched off without encountering a phase transition (for instance by going to high temperatures in an asymptotically free theory), so they should not affect the  $N$ -scaling of the gluon production rates computed in this section. The arguments of this subsection are valid at all orders in perturbation theory; however, experience with counting powers of  $N$  in the 't Hooft limit (e.g. in exactly solvable matrix models) suggests that the powers of  $N$  obtained from this argument will be correct even non-perturbatively. In specific examples we will provide evidence that this is indeed the case in sections 5-8.

### 3.1. Counting Powers of $N$

Consider a connected Feynman graph that describes  $n$  initial gluons scattering into  $m$  final gluons and  $k$  glueballs. The graph in question has  $n + m$  external gluon lines, and includes  $k$  insertions of glueball creation operators such as  $\text{Tr}F_{\mu\nu}F^{\mu\nu}$ . These operators are normalized so that their two point functions are of order  $N^0$  to ensure that they create glueballs with unit probability; this means that each such operator insertion in a Feynman diagram appears with an extra factor of  $1/N$  compared to an insertion of an interaction vertex. The contribution of this graph to the inclusive probability for glueball production is obtained by squaring the graph and summing over all initial and final gluon states. We will now determine the  $N$  dependence of the result of this process.

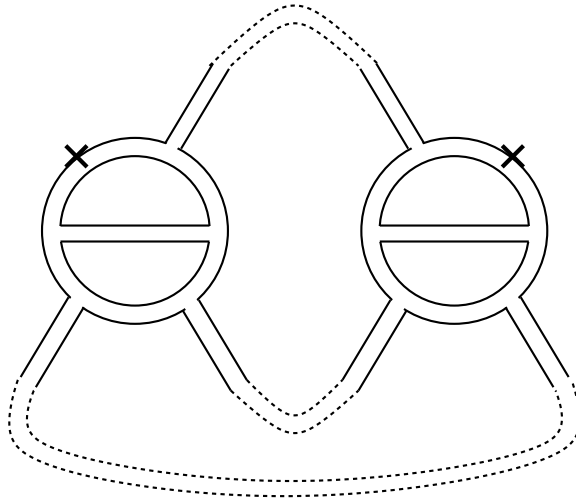


**Figure 2:** A typical sewn graph contributing to the glueball production rate, in double-line notation.

Consider the graph in question, drawn using the 't Hooft double line notation, together with its CPT conjugate (a graph in which fundamental and anti-fundamental indices are interchanged). Sew these two graphs together, as in figure 2, by attaching every free gluon line in the first graph to the corresponding conjugate gluon line in the conjugate graph; this gluing preserves the flow of all color indices. The resulting graph has no free gluon lines, so the faces may be filled in to form a genus  $g$  Riemann surface in the usual manner. The  $N$  dependence of the contribution of this graph to inclusive glueball production is

obtained by freely summing over all indices of the sewn graph<sup>14</sup>, and so is proportional to  $N^{2-2g-2k}$  (using standard 't Hooft counting and the normalization of the glueball creation operators). The leading behavior at large  $N$  is given by planar graphs ( $g = 0$ ) and is proportional to

$$N^{2-2k}. \tag{3.1}$$

### 3.2. $k=0$ : Gluon Mean Free Time

According to (3.1) the effective ‘number’ of gluon-gluon collisions per unit time, in a large plasma-ball of volume  $V$ , is of order  $N^2$ . It follows that the rate at which any given gluon undergoes collisions is of order  $N^0$  (recall that the plasma-ball contains of order  $N^2$  gluons). As a consequence, the relaxation time scale of the plasma fluid is of order  $N^0$ . In appendix C we verify this result at lowest order in perturbation theory.

### 3.3. $k=1$ : Glueball Production Rate

The plasma-ball radiates glueballs by one of two mechanisms. Every once in a while a gluon with indices  $(i, j)$  collides with a gluon with indices  $(j, i)$  near the surface of the plasma-ball; this collision can produce a glueball, which then escapes from the plasma-ball. Alternatively, occasionally an energetic gluon shoots out of the surface of the plasma-ball; the string that attaches it to the plasma-ball can then snap, allowing it to escape into the bulk as a glueball. Glueball production from each of these processes is governed by the Feynman graphs studied in §3.1 above. According to (3.1), in the large  $N$  limit glueball production is dominated by graphs with  $k = 1$ , and takes place at a rate that is independent of  $N$ . In appendix C we study a simple Feynman graph that contributes to glueball production, to verify this conclusion at weak coupling (the general analysis is valid at any value of the 't Hooft coupling).

In this subsection we have focused on the radiation of glueballs from plasma-balls. However the arguments of this section apply equally well to the time reversed process. Consider a glueball incident upon the plasma ball from outside. Equation (3.1) implies

---

<sup>14</sup> This may be argued as follows. Color indices attached to the  $m$  final gluons must be summed over in summing over all final states. Color indices attached to the  $n$  initial gluons must be summed over in summing over all initial gluons – in this step we use the fact that the plasma-ball has a finite density of gluons of any given color variety. All internal color indices must be summed over in squaring the original Feynman graph.

that the interaction cross section for this glueball, per unit length traversed through the plasma ball, is of order  $N^0$ . We expect this interaction process to lead to the glueballs dissolving into the plasma-ball. Similarly, glueballs formed in a gluon collision far from the surface of a large plasma-ball will dissolve before they escape, so the hadronization rate is proportional to the surface area of the plasma-ball rather than its volume.

### 3.4. $k=2$ : Friction

As we have discussed in the previous subsection, the cross section for a glueball traversing the plasma-ball to dissolve into the plasma is of unit order. Glueballs also interact with the plasma in a more elementary manner; gluons incident on the glueball knock it around, slowing down the glueball and causing it to jiggle around as it traverses the plasma-ball. Such interactions are governed by diagrams with one incoming and one outgoing glueball, have  $k = 2$  and so are of order  $1/N^2$ .

## 4. Localized Black Holes in Warped Backgrounds

We now turn to a study of uncharged, static, finite energy (rather than finite energy density) black holes in the backgrounds (1.1), that are localized in the IR region of the radial direction as well as in the  $\mathbb{R}^p$  directions, in the range of parameters where gravity in the background (1.1) is a good approximation to the theory. At low enough energies such solutions are well approximated by ten dimensional Schwarzschild black holes of radius  $R_s \ll \sqrt{\alpha'} L$ , centered at  $u = u_0$  in (1.1). What is the qualitative nature of the static black hole solutions at higher energies? A consideration of the opposite, high energy limit gives us a clue. The confining backgrounds (1.1) host infinite energy translationally invariant (in the field theory  $\mathbb{R}^p$  directions) black brane solutions, which undergo a first order phase transition at some finite temperature<sup>15</sup>. The thermodynamic properties of these black branes are clearly extensive (for instance, their energy is proportional to their volume in  $\mathbb{R}^p$ ). Recall also that the graviton (as well as all other fields) is massive in (1.1); as a consequence all correlation functions decay exponentially in this background. Putting these facts together, it is natural to expect that a black hole whose energy is very large, rather than strictly infinite, is a large spherical lump in  $\mathbb{R}^p$  which in its interior (meaning

---

<sup>15</sup> Note that the deconfinement transition is always of first order when the gravitational approximation is valid, since it occurs far below the Hagedorn temperature which is related to the string tension.

away from its edges in the  $\mathbb{R}^p$  directions – not the black hole interior behind the horizon) closely resembles a translationally invariant black brane. Furthermore, taking the energy and the radius of the lump to infinity and focusing on the edge of the lump, we expect the solution to tend to a planar domain wall interpolating between the confining gravity solution (which is just (1.1)) on one side and the deconfined homogeneous gravity solution (which is the black brane in (1.1)) on the other side.

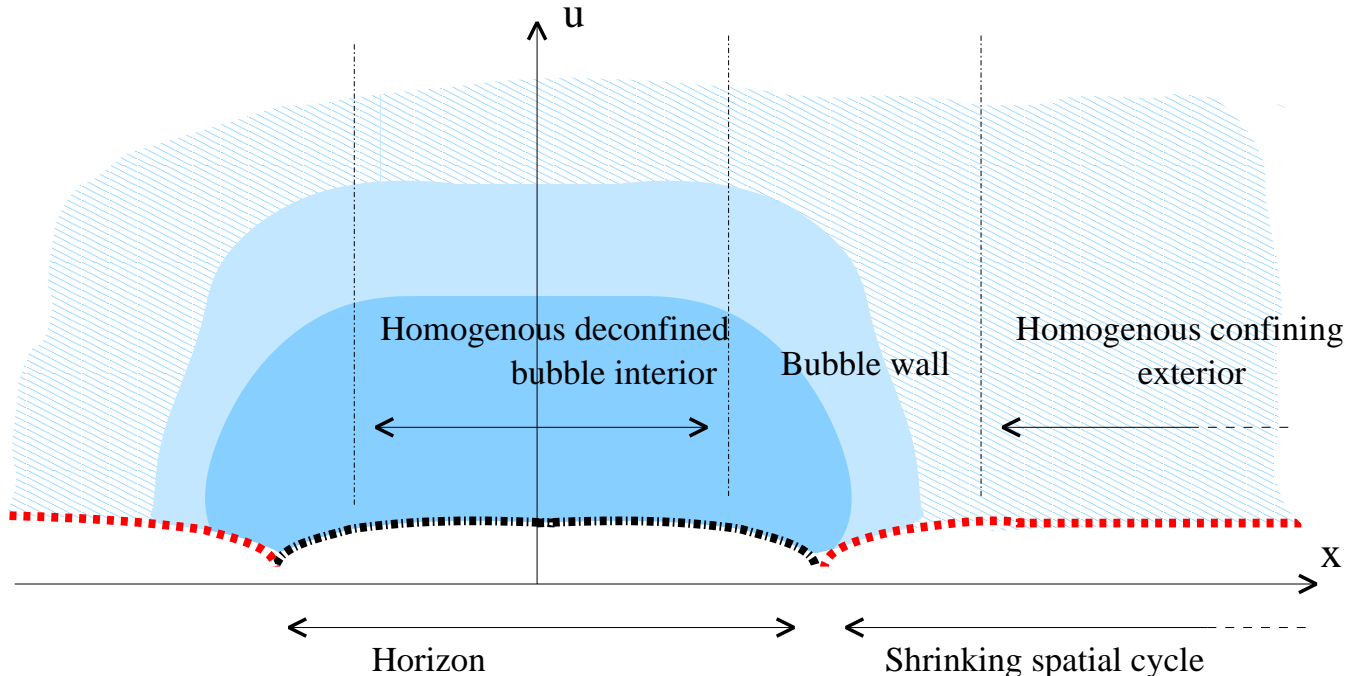


**Figure 3:** The localized black hole. The vertical axis is the radial coordinate, and the horizontal axis  $x$  is one of the spatial  $\mathbb{R}^p$  coordinates.

Of course, uncharged homogeneous black brane solutions exist over a range of temperatures. However, the force balance arguments of §2, which apply to warped backgrounds whenever they possess a well defined boundary stress tensor, tell us that such a large bubble can be static only if the relevant black brane has a pressure that vanishes in the large size limit. This is true for the black brane precisely at the deconfinement temperature (see §2 and appendix A). Indeed, the force balance equation (2.1) is ensured by the conservation of the (boundary) stress-energy tensor (see appendix B.1) which in turn is a direct result of diffeomorphism invariance of the bulk theory in warped gravitational backgrounds (see, for instance, [15,16] and references therein, and see section 8 and appendices E and F for how this works in a specific example). As a consequence, in the classical gravity

approximation (i.e. to leading order in  $1/N$ ), we expect to find large black holes whose interior locally reduces to a homogeneous black brane at the deconfinement temperature. The width of the “domain wall” separating the two regions is expected to be of the order of the curvature scale (which is also the scale of the mass gap in these theories).

Recall that any system undergoing a first order phase transition goes through configurations that consist of bubbles of varying size of one phase inside the other. The pancake-like solutions we have described above are simply increasingly large bubbles of the deconfined phase within the confined phase, except that the confined phase is replaced by the vacuum. Within the classical supergravity approximation the thermal confined phase is indistinguishable from the vacuum (because its energy is  $\mathcal{O}(1)$  rather than  $\mathcal{O}(N^2)$ ), so this last replacement changes nothing. As in section 2, we expect these big black holes to be stable if their surface tension is positive.<sup>16</sup>

Motivated by these considerations, we conjecture that warped backgrounds of the form described in §1.2 always host large pancake-shaped black holes of the form described above (and in the introduction) and depicted in figure 3. In section 8 we will supply evidence for our conjecture by constructing the domain wall that interpolates between the vacuum and the black brane at the deconfinement temperature, in a particularly simple background. We also show that in this specific background the surface tension is positive, so we expect the corresponding black holes to be stable.

Note that the black holes described in this subsection have a finite temperature  $T_d$  in the large mass limit. Moreover, assuming that their surface tension is positive, they have negative specific heat for a rather prosaic reason (see (2.1)); smaller black holes have to be hotter in order to balance the surface tension. Note that this behavior matches smoothly onto the negative specific heat of very small black holes (which should behave like Schwarzschild black holes, see §7.1).

In this section we have focussed on a study of black holes with vanishing angular momentum (and other conserved charges). However, it seems likely that reasoning identical to that presented at the end of section 2 could be used to predict the detailed properties of rotating black holes and black rings (whose horizon contains an  $S^1$  component, similar

---

<sup>16</sup> The domain walls constructed in section 8 do, indeed, have positive surface tension. We are not, however, aware of a rigorous argument that guarantees this will always be the case. If negative surface tension domain walls do exist, we would expect them to possess Gregory-Laflamme like instabilities localized at the surface of the black hole, in analogy with the Gubser-Mitra conjecture [17,18,19].



to the ones of [20]), in the backgrounds studied in this section. We will leave a detailed analysis of such solutions to future work. Here we will merely note that the rotating plasma-ring like solutions described in section 2 exist only when  $p \geq 2$  for the excellent reason that when  $p = 1$  the plasma-fluid has no angular direction in which to rotate. As we have explained, gravitational backgrounds with  $p + 1$  dimensional Lorentz invariant sections, of the form considered in this section, are at least  $p + 3$  dimensional (the two additional dimensions refer to the radial  $u$  coordinate plus the compact part of the internal dimensions, which must be at least one dimensional since some dimensions must shrink in the IR).<sup>17</sup> It follows that an analysis of the sort presented in section 2 predicts black ring solutions only in  $4 + 1$  and higher dimensions. This agrees nicely with the fact that (at least in flat space) black rings do not exist in  $3 + 1$  dimensions, and it predicts that (at least in some gravitational theories) black rings should exist above  $4 + 1$  dimensions.

Similarly, we expect to be able to generalize our solutions by adding charge (global charge in the gauge theory, which maps to a local charge in the gravitational dual). Again we will leave such generalizations to future work. We also expect that there may be phenomenological applications for these localized solutions [21].

## 5. Localized Black Holes as Plasma-balls

We now turn to a dual gravitational description of plasma-ball dynamics in bulk duals of confining large  $N$  gauge theories at large  $\lambda$ . As mentioned in the introduction, there exist several examples of confining gauge theories that have purely gravitational dual descriptions in the large  $\lambda$  limit. Examples include (a specific UV completion of)  $4 + 1$  dimensional super-Yang-Mills theory compactified on a circle with anti-periodic boundary conditions for the fermions [8], “little string theories” (coming from type IIB NS5-branes) compactified on an  $S^2$  [10], and cascading gauge theories [22,9]. The geometries dual to these systems differ qualitatively in several respects<sup>18</sup>; however they all share the general properties described in §1.2. According to the conjecture of the previous section, these backgrounds all possess localized black hole solutions, that closely resemble the deconfined black brane at their center.

---

<sup>17</sup> For example, in the dual of a  $2 + 1$  dimensional confining theory which we will discuss in detail in §8, the ring would be a solution of a  $4 + 1$  dimensional gravitational theory (with negative cosmological constant), with horizon topology  $S^1 \times S^2$ .

<sup>18</sup> This is natural, as the UV dynamics of the various systems differs qualitatively.

A standard entry in the AdS/CFT dictionary identifies the translationally-invariant black brane at any given temperature with the deconfined phase of the dual gauge theory, at the same temperature [8]. It follows that the localized black holes referred to above are dual to localized lumps of plasma at approximately the deconfinement temperature, which are plasma-balls.

In order to build a more detailed dictionary between bulk and boundary degrees of freedom, it is useful to contemplate a Gedanken experiment. Consider a black hole, of the form described in section 4, localized near the origin of  $p$  dimensional space. Imagine scattering a graviton in some mass eigenstate (about the original confining background) off the black hole at a given  $p$  dimensional momentum. The wave-function that describes this scattering process has four components; an incident wave, a reflected wave, a transmitted wave (the part of the wave that stays completely outside the horizon by going around the black hole, including a part going ‘above’ it in the radial direction), and a component of the wave absorbed into the black hole. Each of these components has a natural dual interpretation; a glueball incident on a plasma-ball may be reflected from the ball, transmitted through the ball or may be absorbed into the plasma-ball (thereby dissociating into gluons). We thus conclude that gravitons outside the horizon ‘above’ the black brane region of the localized black hole map to glueballs inside the plasma-ball<sup>19 20</sup>. On the other hand, anything near the horizon (or any possible degrees of freedom behind the horizon) maps to gluon or deconfined degrees of freedom.

As we have already argued in §3, lumps of the deconfined phase have zero overlap with glueballs only at infinite  $N$ . At finite  $N$  lumps of gluon plasma overlap with glueballs; this mixing explains the decay of plasma-balls by hadronization. These statements have a direct gravitational analogue; black holes at finite temperature mix with the gravitons at finite  $g_s$ , a phenomenon that explains the decay of non-extremal black holes by Hawking radiation.

---

<sup>19</sup> Quantum mechanically the momentum of such a graviton fluctuates. The lowest order diagrams that contribute to such fluctuations are of order  $g_s$ , leading to a fluctuation probability of order  $g_s^2 \sim 1/N^2$ , in agreement with the analysis of §3.4.

<sup>20</sup> Gravitons located far in the UV correspond to glueballs that are much smaller than  $\Lambda_{gap}^{-1}$ . Of course, such special glueball configurations have the propensity to expand, which is dual to the propensity of a graviton at large  $u$  to fall into the horizon.

## 6. Plasma-Ball Dynamics from Black Holes

### 6.1. Plasma-Ball Hadronization as Hawking Radiation

We have argued for the existence of stable pancake-like localized black hole solutions in backgrounds of the form (1.1); we have also argued that these black holes are dual to plasma-balls. Of course, these black holes are stable only classically; quantum mechanically they decay via Hawking radiation.

Hawking radiation from the ‘flat’ surface of the pancake (see figure 3), which goes out in the radial direction, is simply reflected back into the black hole (by the effective potential arising from the warp factor in the geometry of (1.1), or, for special modes, by reflecting boundary conditions in the large  $u$  boundary of (1.1)). This fact has a simple interpretation in the dual gauge theory; as discussed in §3, glueballs created by collisions between gluons in the bulk of the plasma-ball dissociate before they are able to escape out of the plasma-ball. The black hole loses energy only from Hawking radiation at its edge, reflecting the fact that only glueballs produced by gluon-gluon collisions near the surface of the plasma-ball can escape.

From a gauge theory point of view, the decay of a plasma-ball is a non-perturbative process that is difficult to study even numerically on the lattice. At large  $\lambda$  the AdS/CFT correspondence maps this hadronization to the quantitatively well understood process of Hawking radiation, permitting a quantitative analysis of decay rates and branching ratios in any model of interest. In particular, this confirms the thermal nature of the decay of the plasma-ball, at least at large  $\lambda$ .

In the field theory analysis adding a finite number of quark flavors does not change the analysis, and the same is true also in the string theory duals. Adding flavors in the duals is done by adding D-branes, and in the ’t Hooft large  $N$  limit with a finite number of D-branes, the D-branes have a very small back-reaction and do not affect any of the qualitative discussion above. Note that the Hawking radiation in this case is expected to be partly into closed string modes (glueballs), such as gravitons, and partly into open string modes (mesons).

### 6.2. Plasma-Ball Production in Hadron-Hadron Collisions

Consider the collision of two stable glueballs (with masses of order  $\Lambda_{gap}$ ) at center of mass energies large compared to  $N^2\Lambda_{gap}$ . In the large  $\lambda$  string theory dual these glueballs map to light modes such as gravitons (or other light fields). Giddings [2] has emphasized

that, at large  $\lambda$ , black hole production saturates the inclusive cross section for graviton collisions at high enough energies (up to numbers of order unity); furthermore, this cross section also saturates the Froissart unitarity bound. We pause to review this argument (closely related to an argument given by Heisenberg in 1952 [23,3] using pions instead of gravitons). An upper bound for the inclusive scattering cross section is easily estimated by assuming that gravitational forces dominate at high enough energies. Then, the force between two colliding particles separated by impact parameter  $b$  may be estimated to be of order  $\frac{G_4 E^2}{b^2} e^{-\Lambda_{gap} b}$ , where we have used the fact that gravity is massive in the relevant backgrounds. Consequently, incident particles simply sail past each other when  $b$  is larger than a number of order  $\ln(E)/\Lambda_{gap}$  (up to corrections that are subleading at large energies), and the inclusive cross section is bounded from above by

$$\sigma \sim \ln^2(E)/\Lambda_{gap}^2. \quad (6.1)$$

However, one may independently use shock wave metrics and singularity theorems to demonstrate that the cross section for black hole formation is of the order of  $\sigma$  in (6.1) [2,3].

As we have explained above, localized black holes map to localized lumps of gluon plasma in the dual field theory. It follows as a prediction of the AdS/CFT correspondence that, at large  $N$  and large  $\lambda$ , two glueballs shot at each other with an impact parameter smaller than  $(\ln(E)/\Lambda_{gap})$  will coalesce into a lump of gluon plasma with a probability close to one when  $E \gg N^2 \Lambda_{gap}$ . This lump of plasma, produced at a rate that saturates the Froissart bound, will typically settle into a very long lived plasma-ball, which proceeds to slowly hadronize over a time scale of order  $N^2$ , in the manner described in the previous subsection. Note that even though the black hole forms with a size of order  $\ln(E)$  in the spatial directions of the field theory, it quickly expands to a size of order  $E^{1/p}$  (when the dual field theory has  $p$  spatial dimensions) for which it can be meta-stable.

The reader may find the picture sketched in the last paragraph clashing with her QCD-trained intuition, which might lead her to expect the fast partonic constituents of the glueball to either pass right through each other or to undergo a small number of hard collisions rather than smoothly coalescing into a plasma-ball. Of course the utility of partonic ideas is questionable at large  $\lambda$  (where partons interact strongly at all energies). Nevertheless, to the extent that this notion is valid, rapid gluon radiation ensures that the

parton distribution function is peaked at small values of  $x$  [14] so that the average parton energy is of order

$$E_{parton} \approx E \left( \frac{\Lambda_{gap}}{E} \right)^\lambda \quad (6.2)$$

where  $E$  is the center of mass energy of the collision, ensuring that  $E_{parton} \ll \Lambda_{gap}$  at large  $\lambda$ , so that glueballs simply do not contain fast partons. Thus, at large  $N$  and large  $\lambda$ , glueball-glueball collisions are conceptually similar to heavy ion collisions, with the large center of mass energy shared between a large number of constituents.

At small  $\lambda$ , as mentioned above, most of the energy of the glueballs is carried by a small number of partons, each of which carries a significant fraction (an energy of order  $E/\ln(E)$ ) of the energy of the glueball (at high energies the partons tend to have smaller values of  $x$  due to asymptotic freedom, but this is a logarithmic effect that does not affect our arguments). These very energetic partons interact weakly; their interactions will not form a plasma. As a consequence we expect a crossover in the dominant behavior of high energy scattering at  $\lambda$  of order one. <sup>21</sup>

It would be interesting (and may be possible) to quantitatively verify the qualitative picture sketched in this subsection.

## 7. Black Hole Physics from Gluon Plasmas

As we have argued above, in confining gauge theories at large  $\lambda$ , black holes in the IR of the background (1.1) are dual to plasma-balls. As discussed below, the decay process of these plasma-balls goes through ten dimensional Schwarzschild black holes. To our knowledge this is the first proposal for the dual of classically stable small black holes (black holes whose size is small compared to the curvature scale of the space that hosts them). As a consequence, we are able to use the setup of this paper to inquire how various mysterious phenomena involving black holes (for instance, the complete absorption of any

---

<sup>21</sup> Note that even at small  $\lambda$  the glueball still contains a large number of small  $x$  partons whose strong interactions might create a lump of gluon plasma. However, this lump will not carry a finite fraction of the center of mass collision energy. One might think that even if only a small plasma-ball is formed, the fast partons would be bound to it by a string (since they carry a color charge) so they would eventually be pulled back into it, given that strings cannot break in the large  $N$  limit. However, since in order to form the plasma we need an energy at least of order  $N^2$ , the fast partons will also carry an energy of order  $N^2$ , allowing the relevant strings to snap even in the large  $N$  limit (since their length would be of order  $N^2$ ).

incident object) manifest themselves from the dual viewpoint. The dual picture also allows us, in principle, to investigate how  $\alpha'$  and  $g_s$  corrections modify the classical properties of black holes. In this section we will present a very preliminary discussion of these extremely interesting questions.

### 7.1. *The Fate of Small Schwarzschild Black Holes*

As the pancake-shaped black holes (at large  $\lambda$ ) lose energy into radiation they shrink in size until their size approaches the curvature length scale of the space (1.1) that hosts them; they then localize on the internal manifold (via a Gregory-Laflamme [17,18] type transition)<sup>22</sup>, and then shrink further until their size is much smaller than the length scale of the background curvature. At this point the black holes resemble ten dimensional Schwarzschild black holes<sup>23</sup>. Thus, the subsequent evolution of these black holes is identical to that of black holes in flat ten dimensional space. As these black holes continue to lose energy by Hawking radiation, they eventually shrink to the string scale; the qualitative nature of their subsequent evolution is of great interest (see appendix D for a discussion).

Of course the slow decay of warped black holes, described in the paragraph above, has a dual description as the decay of plasma-balls (by hadronization) in gauge theories at large  $\lambda$ . The properties of small (string sized) black holes map to the properties of small plasma-balls, a reformulation that may be useful.

### 7.2. *Information Conservation in Hawking Radiation*

It has often been pointed out that the AdS/CFT correspondence ensures that black hole evaporation is a unitary process. Our identification of specific gauge theory configurations (occurring in the decay process of plasma-balls) with ‘small’ ten dimensional

---

<sup>22</sup> Note that such a transition is not expected to occur at small  $\lambda$ , and this may cause some differences between the details of the decay process at small  $\lambda$  and at large  $\lambda$ . Note also that this localization transition may not be smooth, so part of the energy of the black hole may be lost in the transition, but we expect the end-point to be a localized black hole carrying a finite fraction of the initial energy. See [24] for an initial study of the localization transition on  $AdS_5 \times S^5$ . Note that there is still some question whether the Gregory-Laflamme instability leads, in finite time, to an end state with localized horizon [25]. See [26] and references therein for a study of the Gregory-Laflamme transition from a dual gauge viewpoint, in a similar context.

<sup>23</sup> Note that this is true for all known theories with large  $\lambda$ , despite the very different UV physics of these theories. It would be interesting to understand this universality better from the field theory point of view.

Schwarzschild black holes makes this argument more specific. The production of a plasma ball in a glueball-glueball collision, and its subsequent decay via hadronization is clearly a unitary process; the end point of this process is only approximately thermal.

Of course a full resolution of the information paradox requires the identification of the flaw in Hawking’s argument that predicts a breakdown of unitarity. While the dual description of Hawking radiation is manifestly unitary, it has not yet proved possible to formulate Hawking’s argument in gauge theory language in order to identify its flaw. This is an important problem that deserves attention.

### 7.3. *How Black is a Black Hole ?* <sup>24</sup>

It is a striking feature of classical black holes in general relativity (the feature responsible for their name) that a particle squarely incident on the black hole is always absorbed, no matter how large its energy.

In this paper we have identified a black hole with a plasma-ball, a localized lump of gluon plasma at temperature  $T_d$ . It might, at first, seem that a particle incident on the plasma-ball at an energy  $E$  much larger than  $T_d$  would sail right through it (undergoing a series of grazing collisions that hardly affect it), in blatant contradiction with the expectations of black hole physics. We have already explained in subsection 6.2 that this naive expectation is incorrect. The only objects available to be hurled at the plasma-ball are glueballs. At large  $\lambda$  glueballs may be thought of as consisting of a very large number of low energy partons; the average parton energy is  $E_{parton}$  in (6.2). Note that  $E_{part} \ll \Lambda_{gap}$  even in the limit  $E \rightarrow \infty$ . As a consequence, glueballs may always be absorbed by plasma-balls, no matter how high the incidence energy.

As we have explained in subsection 6.2, however, glueballs at small  $\lambda$  are composed dominantly of a small number of high energy partons. We expect that these partons should simply blast through the plasma ball at high enough  $E$  (note that  $E$  may have to be of order  $N$  in order to permit these partons to snap confining strings that may bind them to the plasma-ball and to escape all the way to infinity, since the snapping probability per unit time and unit length of the string is of order  $1/N^2$ ). Thus, plasma-balls at small  $\lambda$  (where string corrections are very important) do not share all the properties of their large  $\lambda$  cousins (in particular they no longer efficiently absorb glueballs).

---

<sup>24</sup> The results of this subsection were obtained in collaboration with Nima Arkani-Hamed.

It is tempting to translate the last paragraph into a statement about a reduction in the absorptive properties of black holes in warped backgrounds whose curvatures are of the order of the string scale. Of course, this translation has an obvious pitfall; a glueball blasting through a plasma-ball may have a more mundane dual description, as a graviton that evades the corresponding black hole by going around it in the radial direction<sup>25</sup> (needless to say, all these notions are a little fuzzy when curvatures are stringy). Nonetheless, this suggestion is intriguing and deserves further investigation.

## 8. Numerical Solutions for Domain Walls in some Specific Backgrounds

### 8.1. Scherk-Schwarz Compactifications of Anti-De Sitter Space

In this section we turn to a detailed study of the specific warped background

$$ds^2 = L^2 \alpha' \left( e^{2u} (-dt^2 + T_{2\pi}(u) d\theta^2 + dw_i^2) + \frac{1}{T_{2\pi}(u)} du^2 \right), \quad (8.1)$$

where  $i = 1, \dots, d-1$ ,  $\theta \equiv \theta + 2\pi$  and

$$T_x(u) = 1 - \left( \frac{x}{4\pi} (d+1) e^u \right)^{-(d+1)}. \quad (8.2)$$

This metric, known as the AdS soliton [28], is a solution to the  $d+2$ -dimensional Einstein equations with a cosmological constant

$$R_{\mu\nu} = -\frac{d+1}{L^2 \alpha'} g_{\mu\nu}, \quad (8.3)$$

and has a simple physical interpretation [8]. It may roughly be thought of as a Scherk-Schwarz compactification of  $AdS_{d+2}$  on a circle. Indeed, at large  $u$ ,  $T_x(u) \simeq 1$  and (8.1) reduces to  $AdS_{d+2}$  in Poincaré-patch coordinates, with  $u$  as the radial scale coordinate, and with one of the spatial boundary coordinates,  $\theta$ , compactified on a circle (the remaining boundary coordinates,  $w_i$  and  $t$ , remain non-compact). At smaller values of  $u$ , (8.1) deviates from the metric of periodically identified  $AdS_{d+2}$ . In particular the  $\theta$  circle shrinks to zero at a finite value of  $u$ , smoothly cutting off the IR region of  $AdS_{d+2}$ .

In order to describe thermal physics about (8.1) it will be convenient to switch to Euclidean space. Compactifying time  $\tau \equiv \tau + \beta$  on the Euclidean continuation of (8.1)

$$ds^2 = L^2 \alpha' \left( e^{2u} (d\tau^2 + T_{2\pi}(u) d\theta^2 + dw_i^2) + \frac{1}{T_{2\pi}(u)} du^2 \right), \quad (8.4)$$

---

<sup>25</sup> This was discussed in a somewhat different context in [27].



we obtain the Euclidean configuration for a thermal gas of gravitons (at temperature  $T = 1/\beta$ ) about (8.1). The background

$$ds^2 = L^2 \alpha' \left( e^{2u} (T_\beta(u) d\tau^2 + d\theta^2 + dw_i^2) + \frac{1}{T_\beta(u)} du^2 \right) \quad (8.5)$$

yields a second smooth Euclidean manifold with the same asymptotics; upon continuing to Lorentzian space this solution has a horizon, so we identify it with the black brane at temperature  $T = 1/\beta$  about (8.1).

It is immediately evident that for  $\beta = 2\pi$  the solutions (8.4) and (8.5) (the thermal gas and the black brane) are identical (they differ only by a labeling of circles) and so have the same free energy. In appendix E we compute the boundary stress tensor and free energy for these two solutions at every temperature, and demonstrate that the thermal gas has lower free energy for  $\beta > 2\pi$ , while the black brane solution dominates the thermodynamics at all higher temperatures. We also explicitly verify that the pressure of the black brane vanishes at the phase transition temperature  $T_d = 1/2\pi$ , as anticipated by the general arguments of section 4.

Fluctuations around (8.1) have a mass gap, and the phase transition temperature is of the same order as the mass gap (both are of order one in our conventions). It is also easy to check that the thickness of the brane at the phase transition temperature (the minimal value of  $u$  in (8.5)) and the confinement scale of massive particles (the exponential decay in the radial direction in solutions of  $\partial^2 \phi = 0$  in the background (8.1)) are both of order one.

Therefore, the background (8.1) is a particularly simple warped background of the form described in subsection 1.2; its simplicity stems partly from the fact that it is a solution to Einstein's equations with a cosmological constant but no additional matter fields. Moreover, the background (8.1) also appears as a component of string compactifications that are dual to interesting field theories, as we now review.

Some backgrounds of the form (8.1)  $\times M$  are solutions of string theory (with appropriate fluxes) that are holographically dual to  $d + 1$  dimensional conformal field theories with one spatial dimension compactified on a circle with anti-periodic (Scherk-Schwarz) boundary conditions for the fermions. When  $d = 3$  the field theory dual to the simplest such compactification (that with  $M = S^5$ ; different choices of  $M$  lead to different field theories) is  $\mathcal{N} = 4$  supersymmetric Yang Mills theory compactified on a Scherk-Schwarz spatial circle [8]. At low energies (and for small  $\lambda$ ) this theory reduces to pure Yang Mills

theory in  $2+1$  dimensions, a confining gauge theory, making contact with the gauge theory discussions in this paper. When  $d = 4$  the field theories dual to such backgrounds are five dimensional superconformal theories compactified on a circle with anti-periodic boundary conditions for the fermionic fields. Such theories are effectively ‘confining’ in four dimensions, and in some cases the corresponding five dimensional conformal field theories may be viewed as the strong coupling limit of a five dimensional gauge theory [29].

For all these reasons, in the next subsection we will turn to a detailed study of the background (8.1). In particular we obtain a numerical construction of the domain wall that interpolates between (8.4) and (8.5) at  $\beta = 2\pi$ .

### *8.2. The Domain Wall: Asymptotic Behaviors*

As discussed in §4, the black hole solutions we are interested in should interpolate between the (Lorentzian versions of the) confining vacuum (8.4) on their outside and the black brane solution (8.5) at the deconfinement temperature on the inside. In the limit that these black hole solutions are very large, the solution in the neighborhood of their edge should reduce to a domain wall (in one of the field theory directions) interpolating between these two solutions.

Since the metrics must depend explicitly on two coordinates (the bulk radial coordinate and the field theory direction normal to the wall), it is unclear whether any analytic solutions may be found. The elegant Weyl metric, whilst extended to higher dimension, has not been extended to include a cosmological constant [30,31,32]. Hence we will use numerical methods to construct the metric, following those employed previously in [33,34,35] (see also [36]). Note that whilst it seems possible that the domain wall system we solve here may one day find an analytic solution, similar equations with more bulk matter, such as that found in general confining dual backgrounds [12,9,10], would likely not be solvable, whereas the numerical methods we set-up here should easily extend to these cases. Furthermore, the finite size black hole problem is likely to remain analytically intractable.<sup>26</sup> We focus our calculation on the domain wall solution rather than on finite size solutions

---

<sup>26</sup> There has been interesting analytic progress in lower dimensional ( $d = 2$ ) cases with just a negative cosmological constant and the bulk ending at a thin brane [37,38]. This progress follows from the AdS C-metric [39], which unfortunately is not known in more than 4 dimensions. We also emphasize that everything we say applies only to warped backgrounds with a mass gap (and with no four dimensional massless gravity). In particular the analysis of this paper may not apply to ‘cut off’ AdS geometries with a massless ‘radion’ field.

simply because the equations and solution are most elegant in this case. Moving to finite size is in principle a straight forward extension of the methods we use, which we leave for future work.<sup>27</sup>

In this subsection we give an overview of our numerical construction of this domain wall. The formal construction, detailing the equations to be solved, the boundary conditions and the data, is presented in appendix F. Numerical details are given in appendix G. We are mostly interested in the cases of  $d = 3, 4$  but we present our formulae for arbitrary dimension. We will consider the problem in the Euclidean setting, although we stress that the equations, and their boundary conditions, are totally independent of the spacetime signature. The static Lorentzian solution is obtained by trivial continuation of the Euclidean one.

We will search for a solution to (8.3) that preserves rotational and translational symmetry in  $(d - 2)$  of the  $(d - 1)$  spatial  $w_i$  directions, which we call  $r_a$  ( $a = 1, \dots, (d - 2)$ ), and translational symmetry in the  $\theta$  and  $\tau$  directions. The background is also required to respect reflection symmetry in  $\tau$  and  $\theta$ . It follows that it is locally possible to choose the metric for our background to take the form

$$ds^2 = A^2 d\tau^2 + B^2 d\theta^2 + e^{2C} dr_a^2 + e^{2D} (dx^2 + dy^2), \quad (8.6)$$

where the metric functions depend on the coordinates  $x, y$  which represent some combinations of the field theory direction on which the domain wall is localized and of the radial coordinate in the bulk space (we choose specific combinations such that the metric takes the form (8.6)). We take the coordinate periodicity of the  $\tau, \theta$  circles to be  $\beta, \tilde{\beta}$  respectively, although we note that in our asymptotic AdS space-time (or, from the perspective of the  $(d + 1)$ -dimensional field theory, due to conformal invariance in the UV) the actual value of  $\beta$  or  $\tilde{\beta}$  is irrelevant. It is only the ratio of the proper size of the Euclidean time circle in the UV to the proper size of the space circle in the UV that is physical. As discussed above, these are equal exactly at the deconfinement temperature and we only expect to find a Euclidean (and hence static Lorentzian) solution in this case.

Note that the ansatz (8.6) leaves a residual diffeomorphism freedom of performing conformal coordinate transformations of the  $x, y$  plane which preserve the form of (8.6).

---

<sup>27</sup> This will introduce new terms in the Einstein equations as planar symmetry in the field theory directions is replaced by spherical symmetry, and similarly the boundary conditions will then include the origin of these spherical-polar coordinates. However the same methods will apply, and in particular the metric will still depend non-trivially on only two coordinates.

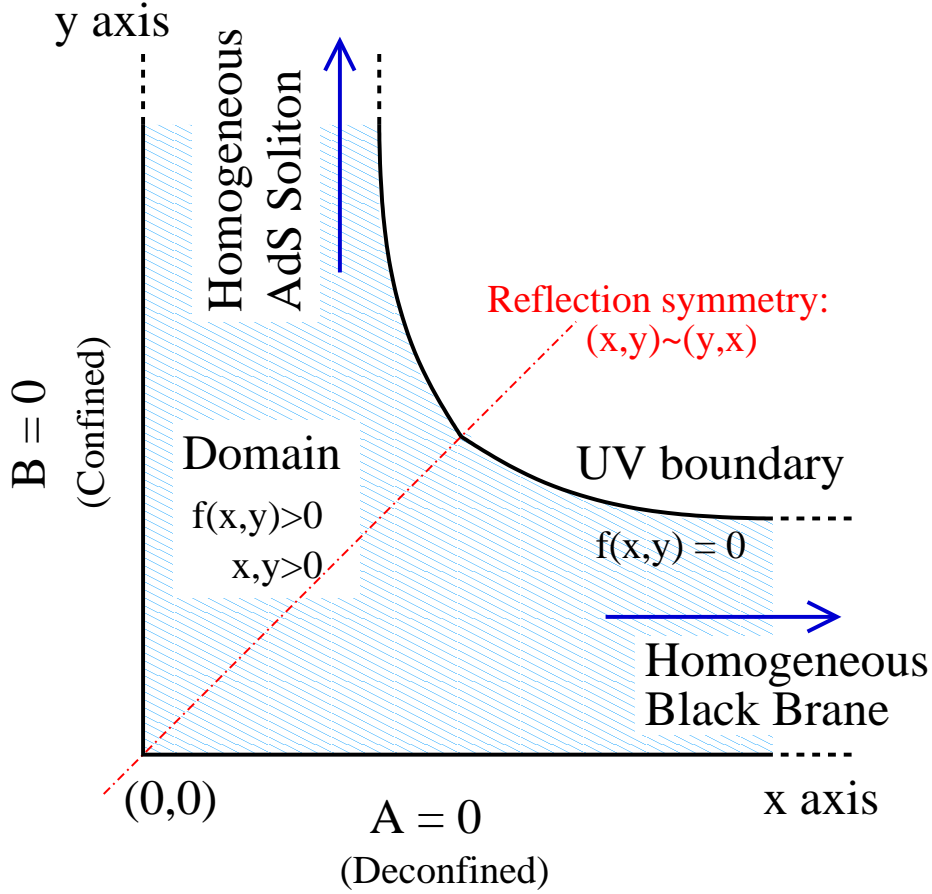


**Figure 4:** Domain of problem in  $x, y$  plane.

Remembering that (non-singular) two dimensional conformal transformations can map any region into any other region (preserving angles at corners), we will use this freedom to position the boundaries of the domain of our coordinates  $x$  and  $y$  as in figure 4. We will take the IR boundaries to be at  $x = 0$  and  $y = 0$ , and the UV boundary will be defined by the vanishing of a function  $f(x, y)$ . For large  $x$  we take the function  $f$  to vanish at  $y = c$ , for some constant  $c$ . For large  $y$ , similarly we take  $f$  to vanish at  $x = c$ . Furthermore we will choose  $f$  so that the function is invariant under the  $\mathbb{Z}_2$  symmetry  $f(x, y) = f(y, x)$  (which will yield a  $\mathbb{Z}_2$  symmetry of our solution, to be discussed below). We regard the locus of the zero of  $f$ , and thus the particular value chosen for  $c$ , to be fixed throughout the following discussion. Note that the particular value of  $c$  chosen is irrelevant, and may be changed simply by performing a global scaling  $(x, y) \rightarrow (\lambda x, \lambda y)$ , which rescales the UV boundary position and the metric functions  $A, B, e^C$  together with  $\beta, \tilde{\beta}$  but does not physically change the solution.

The metric may always be written in the form (8.6) locally. We assume that there exists a solution for which the metric functions  $A, B, C, D$  in (8.6) are finite everywhere in the coordinate domain of the problem, except at the conformal boundary in the UV where  $f$  has a first order zero and  $A, B, e^C, e^D \sim 1/f$ . It is certainly not obvious that such a solution exists, but we will show that it does by constructing it numerically. Note that once we have made the choice of coordinate boundaries above, we have completely fixed the residual conformal coordinate freedom (up to pathological transformations which diverge at large  $x, y$  and thus are projected out under our finite metric component assumption).

Let us discuss the boundary conditions in more detail. The bulk space-time has a conformal boundary at  $f(x, y) = 0$ , and the region near  $f = 0$  looks like anti-de Sitter space near its conformal boundary. Thus the conformal boundary metric is (conformally) flat. We require the bulk to close smoothly in the IR, with either the  $\tau$  or  $\theta$  circles shrinking to zero size. As indicated in figure 4 we choose the time ( $\tau$ ) circle to shrink for  $x > 0, y = 0$  and the space ( $\theta$ ) circle for  $y > 0, x = 0$ . At the origin  $x = y = 0$ , both circles smoothly vanish, as discussed in more detail below. At large  $x$  and at large  $y$  the geometry should tend to one of the homogeneous solutions (8.4) and (8.5) with the appropriate circle shrinking, as detailed in the previous subsection.

The residual conformal transformations that preserve the form of (8.6) and maintain the finiteness of the metric functions must preserve angles at corners of boundaries of the domain. Hence we have made a crucial choice above, namely that the angle between the  $x$  and  $y$  axes is a right angle. Let us now justify this choice. If we focus on a small enough region near the origin in  $x$  and  $y$  we may ignore the bulk cosmological constant. The local geometry here must be flat space, since we require the Euclidean geometry to be smooth. Hence, the metric must take the form

$$ds^2 = \left[ A^2 d\tilde{\tau}^2 + B^2 d\tilde{\theta}^2 + (dA^2 + dB^2) \right] + [e^{2C} dr_a^2] + O(A^2, B^2) \quad (8.7)$$

to leading order in  $A, B$  around  $A = B = 0$ , where to leading order  $C$  is a finite constant, and  $\tilde{\tau}, \tilde{\theta}$  are rescalings of  $\tau, \theta$  with coordinate period  $2\pi$ , such that this Euclidean manifold is smooth. This is simply  $(d + 2)$ -dimensional flat space, written as a product of four dimensional flat space, in double polar coordinates, and the flat  $(d - 2)$ -dimensional space parameterized by the  $r_a$  directions. In (8.7) the lines defined by the shrinking circles,  $A = 0$

and  $B = 0$ , are indeed at right angles, and the metric components are finite, justifying our choice for the IR boundary.<sup>28</sup>

The analytic details of the construction are found in appendix F. There we find that the boundary conditions have no remaining data once we have specified our IR and UV boundary locations (and fixed the trivial rescalings of the  $\tau, \theta, r_a$  coordinates). The equations and boundary conditions in the IR and UV (having chosen appropriately the UV boundary location as described above) are invariant under the  $\mathbb{Z}_2$  symmetry  $(x, y) \leftrightarrow (y, x)$  providing we interchange  $A$  and  $B$ , and the asymptotic solutions (8.4) and (8.5) we expect to find at large  $x$  and at large  $y$  are also exchanged by the symmetry. Hence we expect that the solution for the domain wall will possess this  $\mathbb{Z}_2$  symmetry so that

$$\begin{aligned} A(x, y) &= B(y, x), \\ C(x, y) &= C(y, x), \\ D(x, y) &= D(y, x). \end{aligned} \tag{8.8}$$

For a smooth Euclidean geometry this implies  $\beta = \tilde{\beta}$ , so the time and spatial circles have precisely the same proper size in the UV, and so the Euclidean temperature is indeed exactly at the deconfinement temperature, as discussed in the previous subsection. Alternatively, in the Lorentzian setting, the surface gravity of the horizon, as measured by an IR observer far from the domain wall in the confining region, is directly related to the circle size in that region.

Having fixed the coordinate boundary locations (and fixed the trivial rescalings of the  $\tau, \theta, r_a$  coordinates), we obtain a unique solution for the metric functions  $A, B, C, D$  in both  $d = 3, 4$  with the above symmetry. We may then determine the periodicity  $\beta$  of the two circles from the proper gradient of the vanishing of the  $d\tau^2$  metric component in the asymptotic black brane region (or equivalently, the vanishing of the  $d\theta^2$  component in the confining region). We see in appendix F that the Einstein equations indeed guarantee that

---

<sup>28</sup> Define  $z = A + iB$ , and consider a singular conformal transformation that takes the form  $w = z^p$  near  $z = 0$ , with  $w = \tilde{A} + i\tilde{B}$ . Such a transformation with  $p \neq 1$  will change the angle between the two axes. The new metric will contain the terms  $|w|^{p-1}(d\tilde{A}^2 + d\tilde{B}^2)$  from the Jacobian factor of the transformation, so  $e^{2\tilde{D}} = |w|^{p-1}$ . For  $p \neq 1$  this means  $|\tilde{D}|$  is infinite at  $z = w = 0$ . Hence if we require a metric of the form (8.6) with all the metric functions being finite, we *must* have a right-angle between the axes defined by the shrinking of the Euclidean time circle, and that of the space circle.

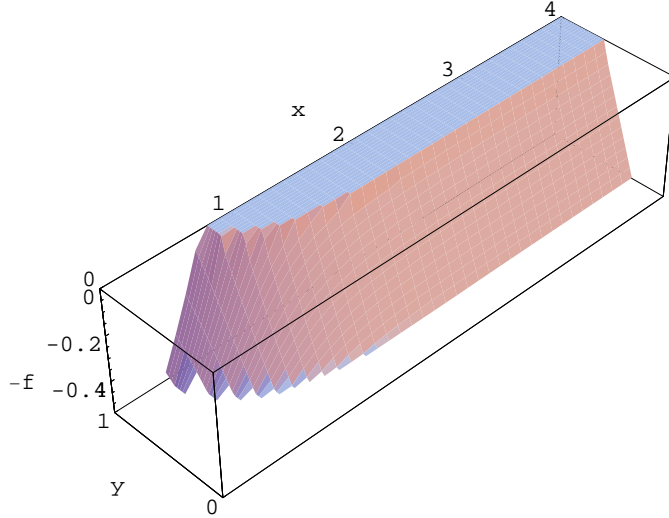


**Figure 5:** Surface plot of  $f$  in the  $x, y$  plane (in fact we plot  $(-f)$  for visual convenience) for  $d = 4$ . The zero of  $f$  gives the position of the UV boundary.  $f$  is not defined over our entire coordinate domain, but rather in a finite region near the UV boundary.

the circle coordinate periods required to smoothly close the appropriate shrinking circle in the homogeneous regions indeed smoothly close the circles everywhere in the solution, in close analogy with the zeroth law of black hole mechanics.

In figures 5 and 6 we present the form of the metric functions we compute numerically for the case  $d = 4$ . For  $d = 3$  their qualitative form is very similar. We work in units where  $L^2\alpha' = 1$ . In figure 5 we show the function  $f$ , whose zero gives the position of the UV boundary. Note that this function is not defined over the entire domain, as it is only required in a neighborhood of the UV boundary. The details concerning the functional form of  $f$  are discussed at length in appendix F. Then, in figure 6 we show surface plots of the metric functions  $A, B, e^C, e^D$  as functions of  $x, y$ . We see that these behave smoothly everywhere, except near the UV boundary where they diverge as  $\sim 1/f$  (where  $f$  has a first order zero).  $A$  goes to zero at  $y = 0$ , and hence the time circle shrinks there. By symmetry,  $B$  goes to zero at  $x = 0$  where the space circle shrinks. We clearly see that at large  $x$  (and by symmetry large  $y$ ) the solution does indeed quickly become homogeneous as expected.

We compute the boundary stress tensor for both the  $d = 3$  and  $d = 4$  solutions in figure 7. The horizontal axis is the proper distance along the boundary (up to a global scaling explained below), which we identify with a coordinate  $g$  in the field theory perpendicular

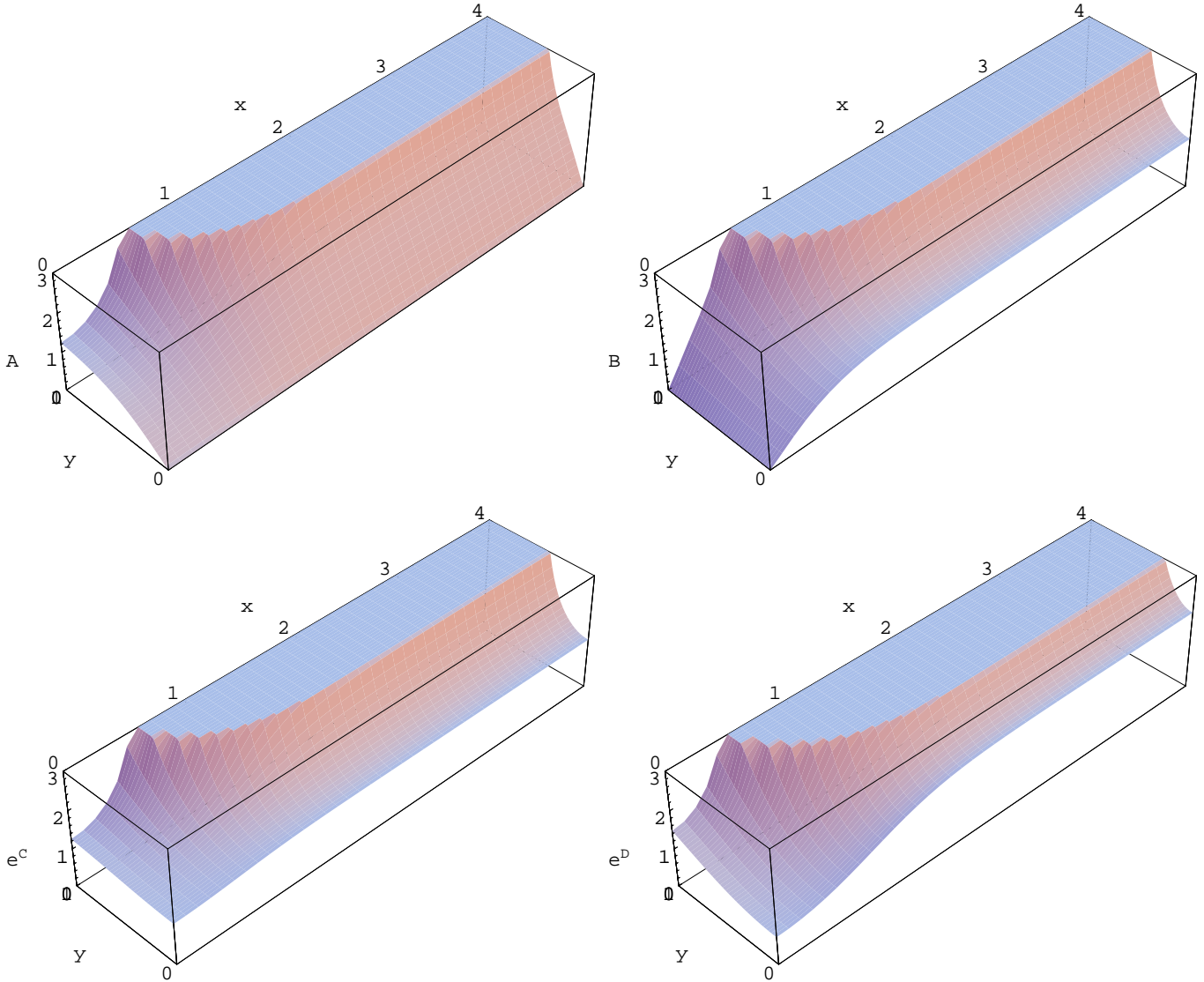


**Figure 6:** Surface plots of  $A$ ,  $B$ ,  $e^C$ ,  $e^D$  in the  $x, y$  plane for  $d = 4$ . The corresponding plots for  $d = 3$  appear very similar.

to the domain wall. The vertical axis gives the various independent components of the traceless stress tensor. A key point is that  $T_{gg}$  is constant (in fact it is zero), since the stress tensor conservation yields  $\partial_g T_{gg} = 0$  (we discuss this in detail in appendix F).

As discussed in appendix B.1, the surface tension of the domain wall is given by

$$\Sigma = \int_{-\infty}^{\infty} dg T_{r_a r_a} \quad (8.9)$$

(no sum over  $a$ ). From our numerical results depicted in figure 7 we find that the domain wall tension  $\Sigma$ , measured in units (as in the figure) of the energy density  $\rho_c$  of the deconfined



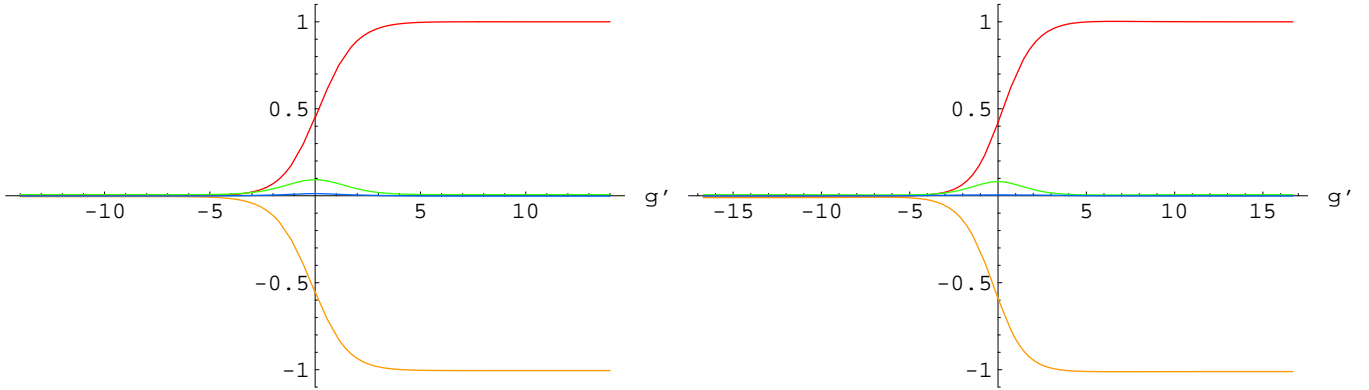


**Figure 7:** The components of the boundary stress tensor (in units where  $T_{\tau\tau} \rightarrow 1$  in the deconfined phase) as a function of a coordinate  $g$  perpendicular to the domain wall (negative is confined region, positive is deconfined region), for  $d = 3$  (left) and  $d = 4$  (right): red (top) =  $T_{\tau\tau}$ , orange (bottom) =  $T_{\theta\theta}$ , green (top middle) =  $T_{r_a r_a}$ , blue (bottom middle) =  $T_{gg}$ .

phase at the deconfinement temperature divided by the deconfinement temperature  $T_d$  (which was used to set the scale of the  $g$  coordinate in figure 7), is given by  $\Sigma = 2.0 \times \rho_c/T_d$  for  $d = 3$  and by  $\Sigma = 1.7 \times \rho_c/T_d$  for  $d = 4$ . We estimate the systematic error in these numbers to be no more than ten percent.

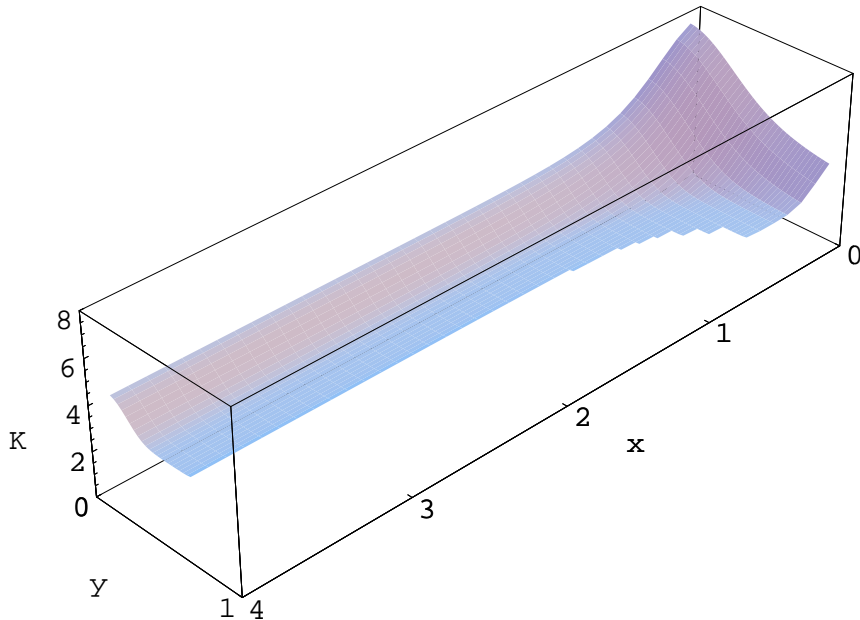


**Figure 8:** Surface plot of the scalar curvature invariant  $K = (R_{\mu\nu\gamma\rho}R^{\mu\nu\gamma\rho})^{1/4}$   $x, y$  plane for  $d = 4$ .

Finally, in figure 8 we plot the scalar curvature invariant  $(R_{\mu\nu\gamma\rho}R^{\mu\nu\gamma\rho})^{1/4}$  for the  $d = 4$  solution. We see that near the UV boundary it tends to a constant, namely that for AdS. In the homogeneous regions it is a little larger in the IR, reflecting the fact the solution is really Euclidean AdS-Schwarzschild, with greater curvature localized where the circle shrinks. In the domain wall region, we see the curvature is increased, but it is everywhere smooth as we expect.

### Acknowledgements

We especially thank N. Arkani-Hamed for collaboration on some stages of this project and for many useful discussions. We thank T. Friedman for suggesting the name plasma-balls. We would like to thank M. Berkooz, R. Bhalerao, M. Douglas, R. Gaii, S. Giddings, R. Gopakumar, D. Gross, S. Gupta, G. Horowitz, V. Hubeny, I. Klebanov, B. Kol, H. Kudoh, D. Kutasov, H. Liu, J. Maldacena, J. Marsano, R. Myers, H. Nastase, C. Nunez, K. Papadodimas, B. Pioline, J. Polchinski, E. Rabinovici, H. Reall, M. Rangamani, S. Ross, H. Schnitzer, N. Seiberg, S. Shenker, A. Starinets, A. Strominger, M. Van Raamsdonk, C. Vafa, S. Wadia, and F. Wilczek for useful discussions. We especially thank K. Rajagopal for several very useful comments and suggestions that have kept us honest. OA would like to thank Harvard University and the Fields Institute for hospitality. SM would like to thank the organizers of the Post-Strings workshop at CERN and the “QCD and string theory” workshop in Santa Barbara for a stimulating environment during the progress of this work. OA and SM would like to thank the Einstein Symposium at the Library of Alexandria, the Third Regional Conference on String Theory in Crete and the Perimeter Institute for hospitality. SM and TW would also like to thank the organizers of the “String Theory” program at the Benasque Center for Science for a wonderfully relaxed atmosphere and hospitality while this work was being completed. The work of OA was supported in part by the Israel-U.S. Binational Science Foundation, by the Israel Science Foundation (grant number 1399/04), by the Braun-Roger-Siegl foundation, by the European network HPRN-CT-2000-00122, by a grant from the G.I.F., the German-Israeli Foundation for Scientific Research and Development, and by Minerva. The work of SM was supported in part by an NSF Career Grant PHY-0239626, DOE grant DE-FG01-91ER40654, and a Sloan Fellowship. TW is supported by NSF grant PHY-0244821.

## Appendix A. Thermodynamics of Large $N$ Gauge Theories

In this appendix we review the thermodynamic properties of large  $N$   $SU(N)$  gauge theories that undergo first or second order deconfinement phase transitions. We discuss explicitly theories having only fields in the adjoint representation (such as pure Yang-Mills theory and its supersymmetric generalizations), but the discussion does not change if we add a finite number of flavors.

### A.1. Local Stability of Homogeneous Configurations

We begin by reviewing the thermodynamic criteria for the stability of a homogeneous system.

Consider any system (like a gauge theory) described by a local field theory. In the micro-canonical ensemble the system is characterized by the energy density  $\rho \equiv E/V$ , and the thermodynamical behavior is determined by the entropy density  $f(\rho)$ ,  $S = Vf(\rho)$ . The effective temperature is given by  $T = 1/(\partial S/\partial E) = 1/f'(\rho)$ . Here we have assumed that the system is homogeneous, but of course the homogeneous configuration does not always maximize the entropy. To see this, divide the system into two pieces, of volume  $\alpha V$  and  $(1 - \alpha)V$ , respectively. Let the energy in the two parts be  $(\alpha + \delta\alpha)E$  and  $(1 - \alpha - \delta\alpha)E$ , respectively.  $\delta\alpha = 0$  corresponds to the homogeneous system; at small non-zero  $\delta\alpha$  the entropy of this system, above that of the homogeneous configuration, is given by

$$\frac{\delta S}{V} = \frac{\delta\alpha^2 \rho^2}{2\alpha(1-\alpha)} \frac{d^2 f}{d\rho^2}. \quad (\text{A.1})$$

Note that  $\delta S$  has the same sign as  $d^2 f/d\rho^2$ . It follows that the homogeneous phase is locally unstable when  $d^2 f/d\rho^2$  is positive. Since  $df/d\rho$  is the inverse temperature of the system,  $d^2 f/d\rho^2$  has an opposite sign from the specific heat of the system. Consequently, we have merely rederived the well-known fact that homogeneous systems with negative specific heat are unstable.

Note also that the pressure of a system is given by  $p = -\partial E/\partial V|_{fixed S}$ . Using  $dS = dVf(\rho) + f'(\rho)(dE - \rho dV)$ , we find that

$$p(\rho) = -\frac{f'\rho - f}{f'} = -F_{free}(\rho), \quad (\text{A.2})$$

where  $F_{free}$  is the free energy density. The velocity of sound squared is given by

$$v_{sound}^2 = \frac{dp}{d\rho} = \frac{-ff''}{(f')^2}. \quad (\text{A.3})$$

It follows that small pressure waves in this homogeneous system are tachyonic (so that the system is dynamically unstable to small perturbations) if and only if  $f'' > 0$ , reiterating the conclusion of this subsection.

## A.2. Density of States in Confining Gauge Theories

We now specialize to the study of a confining large  $N$  Yang-Mills theory that undergoes a first order deconfining transition, and review the behavior of the function  $f(\rho)$  in this class of theories (which may include the models of [8,12,9,10] at various values of  $\lambda$ ). Two interesting mass scales in such theories are  $T_H \sim M_s$ , the Hagedorn temperature of the low energy confining large  $N$  gauge theory (related to the confining string tension  $M_s^2$ ), and the mass gap  $\Lambda_{gap}$ . At large  $\lambda$ ,  $T_H/\Lambda_{gap}$  is proportional to a positive power of  $\lambda$ , while for small  $\lambda$  this ratio is a number of order one.

We first study  $f(\rho)$  at energy densities which are  $\mathcal{O}(N^0)$  (rather than  $\mathcal{O}(N^2)$ ). When  $\rho \ll M_s^4$  the system is well-approximated by a gas of weakly interacting glueballs, a system that has positive specific heat<sup>29</sup>. When the energy density reaches the string scale,  $\rho \gg T_H^4$ , the system is well-described by a gas of weakly interacting strings at approximately the Hagedorn temperature  $T_H$ ,  $f(\rho) \propto \rho/T_H$  (this is a consequence of the exponential or Hagedorn growth in the high-energy density of states  $e^{M/T_H}$ ). Note that  $d^2 f/d\rho^2$  vanishes, indicating marginal stability, when  $\rho \gg T_H^4$ <sup>30</sup>.

Next, we turn to energy densities of order  $N^2$ . We first consider the very high energy limit. At very high energy densities the system is governed by its high-energy ‘fixed point’. This fixed point could, for instance, be a free theory with a number of particle species of order  $N^2$ , or a conformal field theory in four dimensions. In either of these cases  $f(\rho) \propto N^{1/2}\rho^{3/4}$  for  $\rho \gg N^2\Lambda_{gap}^4$ <sup>31</sup>. In this regime the effective temperature grows indefinitely with increasing density and the system has positive specific heat.

We now turn to intermediate energy densities of order  $N^2$ . When the deconfinement transition is of first order, it must occur at a temperature  $T_d$  lower than  $T_H$  (otherwise the deconfinement transition would be a second order transition at  $T_H$ ; clearly it does not make sense for the confining phase to exist at temperatures larger than  $T_H$ ). Thus, there

---

<sup>29</sup> In theories with a single mass scale,  $M_s$  is of order  $\Lambda_{gap}$  and this energy range is pretty boring. However, at large  $\lambda$ ,  $M_s$  is parametrically separated from  $\Lambda_{gap}$  and this energy range is more interesting – typically the density of low mass glueball states grows as a power of the mass (due to Kaluza-Klein modes in extra dimensions), leading to  $f(\rho) \propto \rho^\alpha$  with  $3/4 < \alpha < 1$ .

<sup>30</sup> More precisely, the behavior in this regime depends on the sign of the corrections to the Hagedorn behavior,  $f(\rho) \sim \rho/T_H + \alpha \ln(\rho)$ , but in any case the second derivative is very small for large  $\rho$ .

<sup>31</sup> Some of the large  $\lambda$  theories that we are interested in actually involve more exotic UV ‘fixed points’, which have a different form of  $f(\rho)$  but the same qualitative behavior.

must exist an intermediate regime between the Hagedorn regime and the high-energy-density regime, in which the effective temperature decreases to a value below  $T_d$ . Such a phase obviously has negative specific heat and is unstable<sup>32</sup>. As  $\rho$  increases in this phase, we expect that  $d^2f/d\rho^2$  decreases monotonically, passing through zero at some  $\rho = \rho_0$  of order  $N^2\Lambda_{gap}^4$ , and eventually joining with the negative values of  $d^2f/d\rho^2$  in the high-energy-density phase.

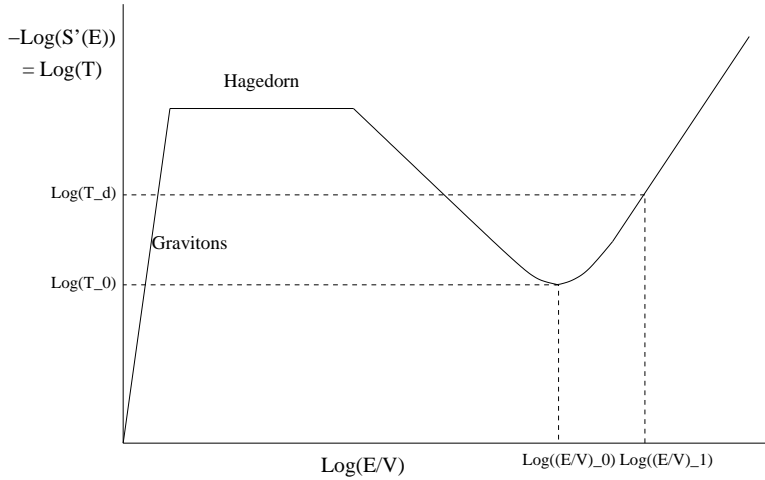


**Figure 9:** The (logarithm of) the effective temperature  $T = 1/(\partial S/\partial E)$  as a function of the (logarithm of) the energy density in large  $N$  confining gauge theories which undergo a first order deconfinement transition.

The behavior described above is depicted in figure 9, which plots the logarithm of the effective temperature as a function of the logarithm of the energy<sup>33</sup>. Stable homogeneous phases correspond to lines with a positive slope in this figure.

The generic behavior of systems exhibiting a second order phase transition is quite similar, except that the unstable intermediate phase does not exist. In such systems the Hagedorn phase joins smoothly with the high-energy-density phase and there is a second order phase transition precisely at the Hagedorn temperature [6,7].

<sup>32</sup> In many gravitational duals at large  $\lambda$ , this phase is dominated by Schwarzschild-like black holes in ten dimensions, for which  $f(\rho) \propto N^{-2/7}\rho^{8/7}$ .

<sup>33</sup> A similar behavior appears also in the gravitational dual of  $(p+1)$ -dimensional conformal field theories compactified on  $S^p$  [40,8]; see [41] for a recent discussion.

### A.3. Phase Separation in Confining Large $N$ gauge theories

Consider the behavior of a large  $N$  gauge theory which has a first order deconfinement transition, at an energy density  $\rho$  which is of order  $N^2$  but smaller than  $\rho_0$ . As discussed above, the homogeneous phase is unstable in this range of densities, so we expect the system to decay into separate regions in two different phases, one with a density smaller than  $\rho$  and the other with a density larger than  $\rho$ . We expect the two phases to be the stable phases in the discussion above, which are the low-energy-density confined phase, at  $\rho < T_H^4$ , and the high-energy-density deconfined phase, at  $\rho > N^2 \Lambda_{gap}^4$ . In the first phase the energy density, entropy density and free energy density are all  $\mathcal{O}(1)$ . We will find it convenient to normalize the extensive quantities (such as  $E$  and  $S$ ) by dividing them by a factor of  $N^2$  as well as by the volume. All normalized extensive quantities vanish in the first phase.

The second phase in this non-homogeneous mixture must have an energy density larger than  $\rho_0$  in order to be stable. We now determine the properties of this phase. Let a fraction  $\alpha$  of the net volume of our system be occupied by this phase; since the energy density of the confined phase is negligible, this means that the energy density in the second phase should be  $\rho/\alpha$ . Now,  $\alpha$  may be determined by maximizing the entropy of the system, which is done by maximizing  $\alpha f(\rho/\alpha)$ . This is the same as maximizing  $S(\rho')/\rho'$ , where  $\rho'$  is the energy density of the second phase. The energy density  $\rho' = \rho/\alpha$  of the second phase is determined by this maximization, which gives the equation

$$f'(\rho') = \frac{f(\rho')}{\rho'}. \quad (\text{A.4})$$

It is not difficult to see that equation (A.4) has a single solution  $\rho_1$ , and that  $\rho_1 > \rho_0$ .<sup>34</sup>

Equation (A.4) may be physically interpreted in several ways. First, recall that the free energy density of our system is given by  $F_{free}(\rho) = (E - TS)/V = \rho - (f(\rho)/f'(\rho))$ .

---

<sup>34</sup> The argument goes as follows. Recall that, for  $\rho < \rho_0$  (but still of order  $N^2$ ),  $f'$  is an increasing function. It follows that, for  $\rho < \rho_0$ ,  $f'(\rho)$  is more than its average value  $(f(\rho)/\rho)$  between 0 and  $\rho$ . Consequently, (A.4) has no solutions for  $\rho < \rho_0$ . Now, for  $\rho$  in the high-energy-density phase, the right-hand side of (A.4) is larger than its left-hand side. Consequently, (A.4) must have at least one solution for  $\rho > \rho_0$ . Let the smallest such solution be  $\rho_1$ . Using the fact that  $f'$  decreases for  $\rho > \rho_1$ , it is easy to argue that no  $\rho > \rho_1$  can obey (A.4). It follows that  $\rho_1$  is the unique solution to (A.4). Note that we assume here that there is only one point where the second derivative of  $f$  vanishes (as in the discussion of the previous subsection); this is true in all known cases, though more complicated possibilities cannot be ruled out.

Comparing with (A.4), we conclude that our system has positive free energy density for  $\rho < \rho_1$  but negative free energy density for  $\rho > \rho_1$ ; the free energy density vanishes at  $\rho = \rho_1$ . As the (normalized) free energy density also vanishes in the first phase, the free energy densities of the two phases are equal when the deconfined phase has  $\rho = \rho_1$ , so we conclude that  $\rho_1$  is the energy density of the gluon plasma just above the deconfinement temperature. Second, recalling that the pressure is simply equal to minus the free energy per unit volume (A.2), it follows that  $p(\rho)$  is negative for  $\rho < \rho_1$  but is positive when  $\rho > \rho_1$ , and the pressure vanishes precisely at  $\rho = \rho_1$ .

The bubbles of gluon plasma at density  $\rho_1$  which appear in this discussion resemble the localized bubbles discussed in section 2; the main difference between them is that the bubbles of section 2 had the vacuum outside them rather than the finite-density confined phase, but this difference is negligible in the large  $N$  limit.

## Appendix B. Properties of Plasma Dynamics

### B.1. The Surface Tension of the Plasma-Ball

The force balance equation (2.1) may be derived from stress energy conservation applied to the plasma fluid in polar coordinates. In  $p$  spatial dimensions the equation  $\nabla^\mu T_{\mu r} = 0$ , for static configurations, reduces to

$$\partial_r T_{rr} + \frac{1}{r} (pT_{rr} - g^{ij}T_{ij}) = 0, \quad (\text{B.1})$$

where  $i, j$  are summed over all spatial coordinates. When the plasma fluid is isotropic  $pT_{rr} = g^{ij}T_{ij}$ , and constant  $T_{rr}$  solves (B.1). In the plasma-ball configuration, however, the stress tensor will not be isotropic near the boundary of the bubble. Integrating (B.1) we find

$$T_{rr}(\infty) - T_{rr}(0) = P(0) - P(\infty) = - \int_0^\infty \frac{dr}{r} (pT_{rr} - g^{ij}T_{ij}), \quad (\text{B.2})$$

where  $P(0)$  and  $P(\infty)$  are, respectively, the pressure in the interior and exterior of the bubble. In the plasma-ball configuration the integral on the right-hand side of (B.2) receives contributions only from the neighborhood of the boundary of the bubble. Comparing with (2.1) we conclude that the domain wall tension (for bubbles that are much larger than the width of the domain wall, which is expected to be of order  $1/\Lambda_{gap}$ , so that  $r$  is approximately constant in the region that contributes to the integral in (B.2)) is given by

$$\Sigma = \frac{1}{p-1} \int_0^\infty dr (g^{ij}T_{ij} - pT_{rr}). \quad (\text{B.3})$$

In the limit of an infinite bubble whose domain wall is transverse to the  $x$  direction, stress energy conservation implies that  $T_{xx}$  is a constant (which vanishes since it is zero in the confined vacuum), and the expression for the domain wall tension reduces to

$$\Sigma = \frac{1}{p-1} \int_{-\infty}^{\infty} dx g^{ij} T_{ij} = \int_{-\infty}^{\infty} dx T_{yy}, \quad (\text{B.4})$$

where  $y$  is any spatial dimension along the surface of the domain wall.

In this paper we have assumed that the effective dynamical surface tension between the confined and deconfined phases is positive near the phase transition temperature. This is true in the specific example analyzed in section 8. However, it may turn out that the effective surface tension is negative in some large  $N$  gauge theories – at least we are unaware of an argument that rules out this possibility. Large plasma-balls will not be stable in such theories – they will be unstable to fragmentation into small plasma-balls (whose size is presumably of order the inverse mass gap). However note that, at least in gauge theories at large  $\lambda$ , small plasma-balls (with  $R \ll 1/\Lambda_{gap}$ ) are always stable as they map to Schwarzschild black holes in the dual gravitational theory.

## B.2. Dynamical Evolution of Lumps of Plasma

Consider a lump of gluon plasma with large volume  $V\Lambda_{gap}^3 \gg 1$ , at an average energy density larger than the critical density. The initial pressure of such a bubble is positive, driving the bubble to expand. As the expansion proceeds, the pressure and temperature gradients inside the bubble tend to even out. In large  $N$  systems that undergo first order transitions we have mentioned in section 2 that the plasma-ball is an attractive fixed point in the space of dissipative fluid flows, and so it will be the equilibrium configuration if we start in its domain of attraction. We believe that the only other stable configurations of plasma fluid are disconnected plasma-balls moving away from each other. It follows that, within fluid dynamics, hot lumps of gluon plasma stabilize into a collection of plasma balls.<sup>35</sup>

We will argue below that we do not expect stable plasma-fluid configurations to exist in systems that undergo second order deconfinement phase transitions. We expect the bubbles of plasma in such systems to expand through the deconfinement transition and to rapidly hadronize.

---

<sup>35</sup> Note that, under some circumstances, it is rather natural for a single lump of gluon plasma to break up into many components. This could happen if, for example, during the process of evolution the local energy density of some part of the fluid were to become low enough such that the local speed of sound squared is negative (it should go below  $\rho_0$ , see appendix A), triggering an instability that results in phase separation.



### B.3. Small Plasma-Balls

As discussed in section 3, plasma-balls shrink as they slowly lose energy by radiating glueballs. According to (2.1) the plasma-ball temperature diverges as its radius goes to zero. However, (2.1) does not apply when  $R < 1/\Lambda_{gap}$ , since the surface tension term does not capture all surface terms for small bubbles (contributions to the energy involving the curvature of the surface and inhomogeneities of the plasma are as important or more important). A more detailed microscopic analysis is needed to determine the properties of small plasma-balls. The strongly coupled nature of the gluon plasma may make this analysis rather difficult; however it could be worth the effort, as small plasma-balls encode very interesting information about black hole physics, as we have argued in §6 and as discussed further in appendix D.

### B.4. Plasma Lumps in Theories with Second Order Deconfinement Transitions

Stable plasma-balls do not exist in theories that undergo second order phase transitions, at least when  $\Sigma$  is positive. While plasma-ball-like configurations of finite radius appear to exist as stable solutions of fluid mechanics (using the arguments of section 2), their surface temperature is higher than the Hagedorn temperature, so they cannot be in an approximate equilibrium in a large  $N$  gauge theory<sup>36</sup>. Note also that in this case asymptotically large plasma-ball-like configurations are unstable even within fluid mechanics, as the specific heat diverges (and so the speed of sound vanishes) at the phase transition point in any second order transition.

### B.5. Plasma-Balls in the Real World ?

A large  $N$  version of QCD may be obtained by coupling  $SU(N)$  pure Yang-Mills theory to (say)  $N_f = 2$  or  $N_f = 3$  light quarks (fermions in the fundamental representation). As we have remarked above, there is good evidence that this theory undergoes a first order deconfinement transition and so possesses plasma-balls at large enough  $N$ . If the phase transition stays of first order as we decrease  $N$ , it seems possible that these meta-stable configurations will continue to exist (albeit with decreasing finite lifetimes).<sup>37</sup>

---

<sup>36</sup> Recall that a hot ball above the Hagedorn temperature immersed into a large  $N$  gauge theory cools instantaneously by radiating glueballs at a rate which diverges in the large  $N$  limit.

<sup>37</sup> Note, however, that in QCD-like theories with  $N_f$  of order  $N$ , plasma-balls would not have long lifetimes even if the phase transition remains of first order, because the number of different meson species that they can emit scales as  $N_f^2$ . See [42] for a recent discussion of the deconfinement transition for large  $N \sim N_f$ .

The expected phase diagram of this theory at  $N = 3$ , i.e. of real world QCD, may be found, for instance, in figure 1 of [43]. The nature of the deconfinement ‘transition’ in this diagram depends crucially on the strength of the chemical potential that couples to baryon number. When the chemical potential is small enough, QCD undergoes a smooth crossover between confining and deconfined behavior; this crossover becomes a strong first order phase transition at large chemical potential. As a consequence, QCD could possess meta-stable plasma-ball-like configurations at large enough baryon density, if the phase boundary surface tension is positive (see [44,45] for closely related discussions). However, meta-stable plasma-ball-like configurations will not exist at low baryon density, for instance at the baryon densities attained in the central rapidity region of the fireball created at RHIC, see [46,47] for reviews.

The rapidity tails of the RHIC fireball, as well as suitable regions of the fireball (if one was produced) in the SPS experiment, or plasmas produced in similar experiments where baryons are heated<sup>38</sup> may have chemical potentials large enough to be in the first order regime. It would be interesting to analyze the relevant data from these experiments for evidence of formation of meta-stable plasma-ball-like configurations, that then decay into hadrons at approximately the phase transition temperature (see [49,50] and references therein for discussions along these lines).

### Appendix C. Counting Powers of $N$ at Lowest Order in Perturbation Theory

In this brief appendix we illustrate the arguments of section 3 by explicitly displaying and computing the  $N$  dependence of sample diagrams that contribute to the gluon mean free path and to the glueball production rate at lowest order in perturbation theory.

#### *C.1. $k = 0$ : Mean Free Path*

We check the result of §3.2 at weak coupling by studying the leading gluon-gluon scattering graphs shown in figure 10. First consider the graph in figure 10(A) for scattering an  $(i, j)$  gluon and an  $(m, n)$  gluon, and let  $m \neq j$  and  $n \neq i$ . This diagram is proportional to  $g^2 N^0 = \lambda/N$ , leading to a collision cross section proportional to  $\lambda^2/N^2$  and so a mean free collision time that is independent of  $N$  (the mean free time is obtained by multiplying the collision cross-section by the density of potential collision targets, whose number scales like  $N^2$ ).

---

<sup>38</sup> See figure 1 of [48] for the location of various experiments on the QCD phase diagram.

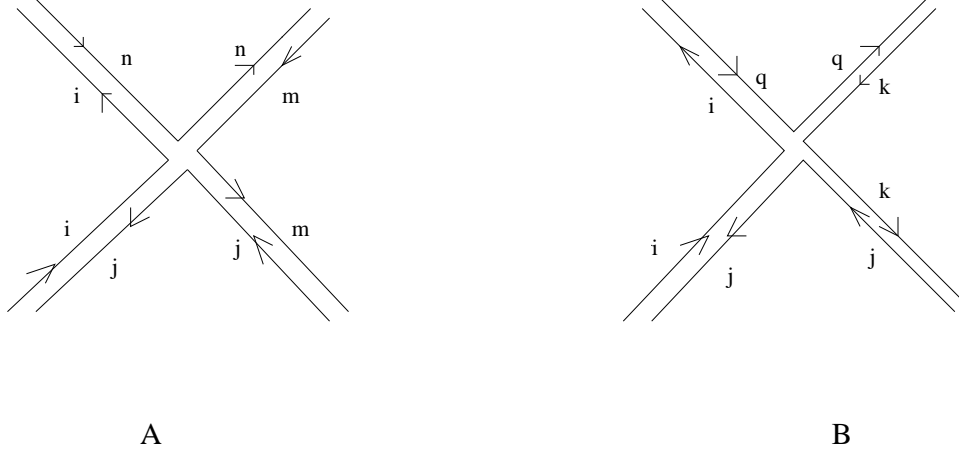


**Figure 10:** Tree diagrams for gluon-gluon scattering in double-line notation.

In the special case that  $(m, n) = (j, k)$  for some  $k$ , the tree-level diagram in figure 10(B) also contributes. The cross section from this diagram is  $\propto \lambda^2/N$ , where the additional factor of  $N$  results from the sum over the  $q$  color index in the final state. This graph too leads to a mean free collision time that is independent of  $N$  as, in this case, the density of potential collision targets scales like  $N$ .

*C.2.  $k = 1$  : Rate of Glueball Production*



**Figure 11:** Tree diagrams for glueball creation by scattering gluons.

Consider glueball production via the gluon-gluon collision depicted on the left of figure 11. The vertex in this graph contributes  $g_{YM}^2$ , the index loop contributes a factor of  $N$ , and the overlap of the two-gluon state with the glueball wavefunction is of order  $1/N$  (this is the  $1/N$  in the normalization of the glueball creation operator), resulting in a collision cross section of order  $1/N^2$ . Multiplying this by the total number of gluons in the plasma-ball, we find a glueball production rate independent of  $N$ .

The same Feynman diagram may be given a different interpretation upon choosing the time slicing on the right of figure 11. This diagram describes an energetic gluon escaping

out of the surface of the plasma, until the string that attaches it to the rest of the plasma snaps by creation of a gluon-anti-gluon pair, allowing the original energetic gluon and its anti-gluon partner to escape away as a glueball. The analysis of the previous paragraph carries through immediately for this process, leading, once again, to a glueball creation rate independent of  $N$ .

## Appendix D. The Final Decay of Small Plasma-Balls

After the black hole/plasma-ball at large  $\lambda$  shrinks such that it resembles a ten dimensional Schwarzschild black hole, it continues to shrink as it evaporates until its proper Hawking temperature is of the order of the Hagedorn temperature  $T_H$  (so that the proper size of the black hole is of order the string scale). At this point the black hole is believed to resemble a highly excited string state [51,52]<sup>39</sup> and there are several possibilities for the subsequent evolution. The black hole could

1. Develop a tachyon (due to stringy  $\alpha'$  corrections) at a temperature smaller than  $T_H$  as a result of which the black hole decays classically, dominantly into low-lying string states (glueballs).
2. Reach the Hagedorn temperature when its mass is of order  $1/g_s^2 \sim N^2$ , at which point it explodes into a gas of dominantly highly excited string states (or transmutes into a single excited long string, depending on details, see for instance section 2 of [7])<sup>40</sup>.
3. Continue to decay thermally (with temperatures less than  $T_H$ ) until its energy is of order one.

Which of the options 1-3 above is actually attained is a question of obvious interest in the study of black hole physics. This question could, in principle, be answered by an investigation of classical string theory, but this has not yet proved possible. Our identification of black holes with plasma-balls allows us to map this question to the properties of small plasma-balls, a reformulation that could lead to progress.

---

<sup>39</sup> See [41] for an intriguing discussion of a possible manifestation of the black-hole excited string transition in  $\mathcal{N} = 4$  Yang Mills on  $S^3$ .

<sup>40</sup> Note that the excited string states are stable in the large  $N$  limit, though for finite  $N$  they would eventually decay into lighter glueballs.

## Appendix E. The Boundary Stress Tensor for Compactifications of $AdS_{d+2}$

Asymptotically  $AdS_{d+2}$  backgrounds possess a conserved  $d + 1$  dimensional stress tensor [53,54,55,56,57]. The stress tensor associated with (8.1) is (see equations 4 and 25 in [58])

$$T_{\mu\nu} = \Theta_{\mu\nu} - \gamma_{\mu\nu}\Theta - (d-1)\gamma_{\mu\nu} = \frac{\alpha e^{-(d-1)u}}{2} (-\delta_{\mu\nu} + (d+1)\delta_{\mu\theta}\delta_{\nu\theta}), \quad (\text{E.1})$$

where the indices  $\mu$  and  $\nu$  run over  $i, t, \theta$ ,  $\gamma_{\mu\nu}$  is the restriction of (8.1) to a constant  $u$  slice,  $\Theta_{\mu\nu} = -\frac{1}{2} \frac{1}{\sqrt{g_{uu}}} \frac{d\gamma_{\mu\nu}}{du}$  and  $\alpha = (d+1)^{-(d+1)}$ . The boundary field theory stress tensor associated with (8.1) is obtained by multiplying (E.1) by  $e^{(d-1)u}$ , so that

$$T_{\mu\nu}^{\text{confined vacuum}} = \frac{\alpha}{2} (-\delta_{\mu\nu} + (d+1)\delta_{\mu\theta}\delta_{\nu\theta}). \quad (\text{E.2})$$

The boundary stress tensor for the black brane solution (8.5) is obtained similarly, giving,

$$T_{\mu\nu}^{\text{black brane}} = (2\pi T)^{d+1} \frac{\alpha}{2} (-\delta_{\mu\nu} + (d+1)\delta_{\mu t}\delta_{\nu t}). \quad (\text{E.3})$$

The subtraction we used to define the stress tensor in (E.1) is the standard subtraction for the  $(d+1)$ -dimensional field theory, which gives a vanishing stress tensor in the vacuum of this theory. From the point of view of the  $d$ -dimensional field theory which we obtain after compactifying on the circle, it is more natural to use a different subtraction in which the stress tensor in the vacuum (8.1) of this theory evaluates to zero. Performing the necessary subtraction we find

$$T_{\mu\nu}^{\text{black brane-sub}} = \frac{\alpha}{2} \left[ -((2\pi T)^{d+1} - 1) \delta_{\mu\nu} + (d+1) \left( (2\pi T)^{d+1} \delta_{\mu t}\delta_{\nu t} - \delta_{\mu\theta}\delta_{\nu\theta} \right) \right]. \quad (\text{E.4})$$

In particular, the energy density  $\epsilon$ , free energy density  $f$  and pressure  $P$  of the black brane (the deconfined phase) are given as functions of temperature by

$$\epsilon = \frac{\alpha}{2} (d(2\pi T)^{d+1} + 1); \quad P = -f = \frac{\alpha}{2} ((2\pi T)^{d+1} - 1). \quad (\text{E.5})$$

## Appendix F. Numerical Construction of the Domain Wall Solution

### F.1. Equations and Constraints

Working in units with  $L^2\alpha' = 1$ , the metric we require is Einstein and must solve

$$R_{\mu\nu} = -(d+1)g_{\mu\nu}. \quad (\text{F.1})$$

In our coordinate system (8.6) the three equations from the  $\tau\tau$ ,  $\theta\theta$  and  $r_a r_a$  components manifest the elliptic nature of the static Einstein equations, where the second derivatives are simply the flat two dimensional  $(x, y)$ -Laplacian, giving coupled second order equations for  $A, B, C$ . The equation for  $A$  is

$$\nabla^2 A = (d+1)Ae^{2D} - \left( (d-2)\nabla C + \frac{\nabla B}{B} \right) \cdot \nabla A, \quad (\text{F.2})$$

and the equation for  $B$  is identical after the substitution  $A \leftrightarrow B$  above, since in the static context there is no physical difference between the Euclidean time circle and the compact spatial circle  $\theta$ . The equation for  $C$  is of a similar form,

$$\nabla^2 C = (d+1)e^{2D} - \left( (d-2)\nabla C + \frac{\nabla A}{A} + \frac{\nabla B}{B} \right) \cdot \nabla C. \quad (\text{F.3})$$

The last elliptic (i.e. Laplacian second derivatives) equation can be found for the final function  $D$  from the  $xx + yy$  component of (F.1),

$$\nabla^2 D = -\frac{(d+1)(d-2)}{2}e^{2D} + (d-2) \left( \frac{(d-3)}{2}\nabla C + \frac{\nabla A}{A} + \frac{\nabla B}{B} \right) \cdot \nabla C + \frac{1}{AB}\nabla A \cdot \nabla B. \quad (\text{F.4})$$

The remaining Einstein equations, namely the  $xy$  and the  $xx - yy$  components of (F.1), do not have elliptic second derivatives (but rather  $\partial_x \partial_y$  and  $\partial_x^2 - \partial_y^2$  respectively) and should best be thought of as constraints associated with the gauge-fixing performed in (8.6). Let us write them as

$$\begin{aligned} \alpha &\equiv \sqrt{\det g_{\mu\nu}} (R^x_y) = 0, \\ \beta &\equiv \frac{1}{2}\sqrt{\det g_{\mu\nu}} (R^x_x - R^y_y) = 0. \end{aligned} \quad (\text{F.5})$$

The two non-trivial contracted Bianchi identities then relate  $\alpha$  and  $\beta$  as a very elegant Cauchy-Riemann problem,

$$\begin{aligned} \partial_x \alpha + \partial_y \beta &= 0, \\ \partial_y \alpha - \partial_x \beta &= 0, \end{aligned} \quad (\text{F.6})$$

provided that the above elliptic equations, (F.2), (F.3) and (F.4), are satisfied.

Our strategy in finding solutions will be to solve the elliptic equations, subject to boundary data that ensures that the Cauchy-Riemann problem (F.6) only has the trivial solution  $\alpha = \beta = 0$ , and hence the constraint equations (F.5) will be satisfied. The natural data to take for these elliptic equations is to specify a Dirichlet or Neumann (or mixed) condition on each boundary for each metric function.

## F.2. The IR Boundary Conditions

We now consider the boundary conditions on the IR coordinate boundary where the  $\tau$  or  $\theta$  circle shrinks. Since these two circles are identical from the point of view of the equations, let us choose to discuss the shrinking  $\tau$  circle at  $y = 0$  (the other case being identical with  $x \leftrightarrow y$  and  $A \leftrightarrow B$ ).

There are two sources of data for the functions  $A, B, C, D$ . Firstly, the shrinking cycles imply regular singular behavior in the elliptic equations, and our choice that these metric components be finite singles out certain boundary conditions. Secondly, the constraint equations  $\alpha = 0, \beta = 0$  also lead to boundary conditions.

Firstly, consider the boundary conditions from the elliptic equations at  $y = 0$ . By construction we impose the Dirichlet data  $A = 0$ . When  $A \rightarrow 0$ , some terms in the ‘sources’ for these elliptic equations (F.2), (F.3) and (F.4) are potentially singular, as they go as  $1/A$ . Regularity therefore imposes Neumann boundary conditions on  $B$  and  $C$ ,

$$\begin{aligned}\partial_y B &= 0, \\ \partial_y C &= 0,\end{aligned}\tag{F.7}$$

at  $y = 0$ . Secondly, consider the constraints at  $y = 0$ . These give,

$$\begin{aligned}\alpha : \quad \partial_x (e^{-D} \partial_y A) &= 0, \\ \beta : \quad \partial_y D &= 0.\end{aligned}\tag{F.8}$$

We may immediately recognize the  $\alpha = 0$  constraint as the zeroth law of black hole mechanics. Similarly, for the spatial circle shrinking on  $x = 0$ , it ensures that the geometry will close smoothly for one value of the circle coordinate period.

Note that these boundary conditions are derived from the equations of motion, and are totally independent of whether we work in the Euclidean or Lorentzian setting.

Solving the elliptic equations in an elliptic manner we require one piece of data on each boundary for each metric function. Thus we see that we now have an over-complete set of boundary conditions for  $A, B, C, D$  in the IR. We therefore choose to impose only the  $\beta = 0$  constraint, and hence obtain the rather simple Neumann and Dirichlet data,

$$\begin{aligned}A &= 0, \\ \partial_y B &= 0, \\ \partial_y C &= 0, \\ \partial_y D &= 0,\end{aligned}\tag{F.9}$$

at  $y = 0$ , and similarly for the coordinate boundary at  $x = 0$  the same with  $x \leftrightarrow y$  and  $A \leftrightarrow B$ . We leave the  $\alpha = 0$  constraint to be imposed via the constraint system, by choosing data appropriately on the other boundaries.

An important point is that at the phase interface  $x = y = 0$  both constraints are satisfied automatically due to the factor of  $AB$  occurring in  $\sqrt{\det g_{\mu\nu}}$ . The two constraints take the form,

$$\begin{aligned}\alpha &= A \alpha_{x=0} + B \alpha_{y=0} + AB \alpha_{remainder}, \\ \beta &= A \beta_{x=0} + B \beta_{y=0} + AB \beta_{remainder},\end{aligned}\tag{F.10}$$

where  $\alpha_i, \beta_i$  are linear functions in derivatives of  $A$  and  $B$ , but are not explicit functions of  $A$  and  $B$  themselves. The terms  $\alpha_{y=0}, \beta_{y=0}$  give the constraints (F.8) on the  $y = 0$  shrinking time circle boundary, but do not contribute to the shrinking space circle boundary  $x = 0$  due to the prefactor of  $B$  (omitted in (F.8)). Likewise  $\alpha_{x=0}, \beta_{x=0}$  give the constraints for the shrinking circle boundary  $x = 0$ , and don't contribute to the  $y = 0$  boundary. The final terms  $\alpha_{remainder}, \beta_{remainder}$  contribute to neither boundary as  $AB$  is zero on both, and also at the interface. Hence no additional data is required to satisfy the constraint system at the interface, beyond (F.8) (and its symmetric counterpart at  $x = 0$ ).

### F.3. The UV Boundary Conditions

The UV boundary resides at the locus  $f = 0$  where we demand that the metric looks like the boundary of AdS space, with  $A, B, e^C, e^D \sim 1/f$  (assuming that  $f$  has a first order zero). In order to impose this boundary condition, near the UV boundary we write (8.6) in the form

$$ds^2 = \frac{1}{f^2} (T^2 d\tau^2 + U^2 d\theta^2 + e^{2S} dr_a^2 + e^{2R} |\nabla f|^2 (dx^2 + dy^2))\tag{F.11}$$

and we take the new metric variables  $T, U, S, R$  (which are trivially related to  $A, B, C, D$  via  $f$ ) to be finite there. Coupled with the form above, we also make the further choice that the function  $f$  obeys the Laplace equation

$$(\partial_x^2 + \partial_y^2) f = 0,\tag{F.12}$$

and is defined in a finite neighborhood of the UV boundary. Note that this is consistent with the fact that for large  $x$  we expect  $f \propto (y - c)$ , and  $f \propto (x - c)$  for large  $y$ . The reason for choosing  $f$  to be harmonic is that then we can easily map (F.11) to

$$ds^2 = \frac{1}{f^2} (T^2 d\tau^2 + U^2 d\theta^2 + e^{2S} dr_a^2 + e^{2R} (df^2 + dg^2))\tag{F.13}$$



where the metric components are now written as functions of  $f(x, y)$  and  $g(x, y)$ , with the coordinate  $g$  defined by the Cauchy-Riemann relations,  $\partial_x f = \partial_y g$  and  $\partial_y f = -\partial_x g$ , so that the new coordinates  $f, g$  are conformally related to  $x, y$ . Since  $f = 0$  at the UV boundary, it can be thought of as the asymptotic bulk radial coordinate (like  $u$  earlier), and  $g$  is naturally then the coordinate along the boundary at this zero of  $f$ .

In the coordinates (F.13) it is easy to see that AdS space is simply given by  $T, U, e^S = \text{constant}$  and  $e^R = 1$ , since then the metric (F.13) is just AdS written in the usual Poincaré coordinates. Hence,  $T, U, e^S$  going to constants and  $e^R \rightarrow 1$  near  $f = 0$  will reproduce asymptotically AdS space. Reversing the argument, starting with AdS in Poincaré coordinates near the boundary and choosing our coordinate system (8.6) and the position of the UV boundary to be fixed on some curve  $f(x, y) = 0$ , then the most general form that the asymptotically AdS region can take is (F.11), with  $T, U, e^S = \text{constant}$  and  $e^R = 1$ , for some harmonic function  $f$  with the correct zero locus.

We now make the further choice that

$$T, U, e^S, e^R \rightarrow 1 \tag{F.14}$$

as  $f \rightarrow 0$ , for some given  $f$ , so that the metric of the dual field theory, in the conformal frame defined by  $f$ , is just

$$ds_{d+1}^2 = d\tau^2 + d\theta^2 + dr_a^2 + dg^2. \tag{F.15}$$

This choice is always possible, as we may independently rescale the  $\tau, \theta$  and  $r_a$  coordinates without effecting the Einstein equations. It is this choice (together with the choice of UV coordinate boundary location) that will set the actual values of  $\beta, \tilde{\beta}$  required to smoothly close the manifold in the IR. Note that we have chosen the asymptotic values of  $T, U$  to be the same in order to preserve the natural  $\mathbb{Z}_2$  symmetry of the solution.

Suppose that for some metric  $A, B, C, D$  we choose a particular  $f$  satisfying (F.12) such that the behavior (F.14) is true. Now let us consider a different  $f$ , say  $f'$ , which shares the same locus for its zero, and also satisfies (F.12). Then the induced  $T', U', S', R'$  using  $f'$  will not satisfy (F.14), but rather will go as,

$$\begin{aligned} T', U', e^{S'} &\rightarrow \phi(g) = \frac{|\nabla f'|}{|\nabla f|}, \\ e^{R'} &\rightarrow 1. \end{aligned} \tag{F.16}$$

This gives a boundary metric in the conformal frame defined by  $f'$  which is

$$ds_{d+1}'^2 = \phi(h)^2 (d\tau^2 + d\theta^2 + dr_a^2 + dh^2) \quad (\text{F.17})$$

with  $dg' = \phi dh$ . Hence, different choices of  $f$ , together with the condition (F.14), pick out conformally related boundary metrics, where the normal gradient of  $f$  to its zero determines the conformal scaling.

Thus we could pick a particular  $f$  and implement the freedom of the conformal factor in the asymptotic behavior directly (as in (F.16)). However this considerably complicates the asymptotic behavior of the metric functions. Instead, we do not pre-determine  $f$ , but impose the choice (F.14) and then this scalar degree of freedom is just the normal gradient of  $f$  to its zero.

For any  $f$  satisfying (F.12), the ‘elliptic’ Einstein equations for  $T, U, e^S, e^R$  given by (F.2), (F.3) and (F.4), then yield the following simple behavior near  $f = 0$  :

$$\begin{aligned} T &= 1 + f^{d+1}\delta(g) + f^{d+2}\tau_{d+2}(g) + f^{d+3}\tau_{d+3}(g) + \dots, \\ U &= 1 + f^{d+1}\gamma(g) + f^{d+2}u_{d+2}(g) + f^{d+3}u_{d+3}(g) + \dots, \\ e^S &= 1 - \frac{1}{(d-2)}f^{d+1}(\delta(g) + \gamma(g) + 2\rho(g)) + f^{d+2}s_{d+2}(g) + f^{d+3}s_{d+3}(g) + \dots, \\ e^R &= 1 + f^{d+1}\rho(g) + f^{d+2}\sigma(g) + f^{d+3}r_{d+3}(g) + \dots, \end{aligned} \quad (\text{F.18})$$

where again  $g$  is a coordinate normal to  $f$  which measures the position along the locus of the zero of  $f$ . The four leading ones in these expansions should be likened to Dirichlet data, and as discussed above, guarantee that this geometry is asymptotic to AdS.<sup>41</sup> The four undetermined finite functions  $\delta, \gamma, \rho, \sigma$  should be regarded as Neumann data for the elliptic equations. Since we fix the Dirichlet data, we are not at liberty to also fix these functions when solving the system in an elliptic manner, and these will be determined

---

<sup>41</sup> Choosing the three leading (Dirichlet) terms in the asymptotic expansions of  $T, U, e^S$  to be finite functions of  $g$  (rather than one as in (F.18)) represents a ‘non-normalizable’ deformation of the asymptotic region of the space away from AdS, and will give a non-flat boundary metric. The fourth piece of Dirichlet data is implicit in the finiteness of  $R$  at the UV boundary. Whilst  $e^R \rightarrow 1$  if  $R$  is finite, there is an additional possible non-normalizable behavior, seen most easily in the linear theory where  $R \rightarrow r(g)\log(f)$  is also possible. This can simply be understood as arising from a conformal coordinate transformation moving the coordinate position of the UV boundary, and hence being singular in  $R$ . This function  $r(g)$  which we have implicitly set to zero in (F.18) is the fourth and last piece of Dirichlet data for the functions  $T, U, S, R$  at the UV boundary.

implicitly by the IR boundary conditions. The functions  $\{\tau, u, r, s\}_i$  for  $i \geq d+2$  are terms in the power-series expansion of the metric in  $f$  which are determined in terms of these leading ‘Dirichlet’ and ‘Neumann’ coefficients as in the usual Fefferman-Graham expansion [59,60].

Using these expansions we may compute the boundary stress tensor as in appendix E, with components given by

$$\begin{aligned}
T_{\tau\tau} &= (d+1)\delta(g) + \rho(g), \\
T_{\theta\theta} &= (d+1)\gamma(g) + \rho(g), \\
T_{r_i r_i} &= -\frac{1}{(d-2)} ((d+1)(\delta(g) + \gamma(g)) + (d+4)\rho(g)), \\
T_{gg} &= (d+2)\rho(g)
\end{aligned}
\tag{F.19}$$

in an appropriate normalization. Note that, as required, this is traceless. Recall that we should subtract the confining vacuum stress tensor in order to obtain the standard dual field theory stress tensor. In the flat boundary metric, the conservation equation of the stress-energy tensor gives  $\partial_g T_{gg} = 0$ , and this is crucial in order to understand the pressure balance argument which singles out a particular temperature thermal bubble interior. In the gravity context this arises as a result of the equation of motion of  $G^f_g$ , as we now discuss.

So far we have only discussed the behavior of the ‘elliptic’ equations. Now we evaluate the constraint equations  $\tilde{\alpha} = 0$ ,  $\tilde{\beta} = 0$ , in the new coordinates  $f, g$  :

$$\begin{aligned}
\tilde{\alpha} &\equiv \sqrt{\det \tilde{g}_{\mu\nu}} (R^f_g) = 0, \\
\tilde{\beta} &\equiv \frac{1}{2} \sqrt{\det \tilde{g}_{\mu\nu}} (R^f_f - R^g_g) = 0.
\end{aligned}
\tag{F.20}$$

We note that  $\tilde{\alpha}, \tilde{\beta}$  are simply linearly related to  $\alpha, \beta$ , the coefficients depending on the (non-singular) coordinate transformation between the  $f, g$  and  $x, y$  coordinates. Using the expansion (F.18) we find that both these constraints are finite near  $f = 0$ , although neither is automatically zero, with

$$\begin{aligned}
\tilde{\alpha} &= \frac{d(d+3)}{(d-1)} \partial_g \rho(g) + O(f), \\
\tilde{\beta} &= (d+2) \sigma(g) + O(f).
\end{aligned}
\tag{F.21}$$

We focus on the  $\tilde{\alpha} = 0$  constraint, which is particularly elegant as it implies that  $\rho(g)$  is a constant, say  $k$ , and hence contours of  $f$  and  $R$  are aligned asymptotically. Thus it implies that near the zero of  $f$ ,

$$R(f, g) = kf^{d+1} + O(f^{d+2}). \quad (\text{F.22})$$

Furthermore, this obviously guarantees that  $T_{gg} = \text{constant}$  in the boundary stress tensor (and will be zero with a suitable vacuum subtraction). Note that the actual value of  $k$  is unphysical since in the definition of  $f$  via (F.11) we see the physical metric is invariant under rescalings of  $f$ , while appropriately rescaling the  $\tau, \theta$  and  $r_a$  coordinates too. Therefore we may choose any value for  $k$  that is convenient.

#### *F.4. Solving the Constraint System*

At large  $x, y$  we expect our solution to return to the homogeneous black brane (8.5) or to the AdS soliton (8.4) (this should occur exponentially fast in proper distance, since the effective dual theory has a mass gap). Since the  $\alpha = 0$  constraint is satisfied for a homogeneous solution (depending only on  $x$  or  $y$ ), at large  $x, y$  where the solution should become homogeneous it will quickly go to zero. By the Cauchy-Riemann constraint relations (F.6)  $\beta$  must then go to a constant, and since we are actually imposing  $\beta = 0$  on the IR coordinate boundary, it will also vanish. Hence, the constraints will be satisfied in these asymptotic regions. In the IR we have explicitly imposed  $\beta = 0$  on the axes  $x = 0$  and  $y = 0$ . This is still not sufficient data to solve the constraint problem.

In order to solve the system we could try to impose  $\alpha$  in the IR, but as we discussed above, the elliptic system is already completely determined there. Instead, we may impose the vanishing of some linear combination of  $\alpha$  and  $\beta$  in the UV. With  $\beta = 0$  in the IR, and a linear combination being zero in the UV, combined with the correct large  $x, y$  asymptotics, this is sufficient to guarantee that the solution of the Cauchy-Riemann system (F.6) is such that both  $\alpha$  and  $\beta$  vanish everywhere.

From the discussion above, the natural combination of  $\alpha$  and  $\beta$  to impose is exactly  $\tilde{\alpha}$ , coming from the  $fg$  component of the Einstein equations in the UV, which implies the relation (F.22). Now we already have Dirichlet data for  $T, U, S, R$  in the UV, determined by leading behavior in (F.18), and we cannot also fix the Neumann terms  $\delta, \gamma, \rho, \sigma$ . The only undetermined quantity is the choice of our harmonic function  $f$ . Thus, we impose the constraint  $\tilde{\alpha} = 0$  in the UV by choosing  $f$  to have the correct normal gradient solving (F.22) on its zero locus, so

$$|\nabla(f^{d+1})| = \frac{1}{k} |\nabla R| \quad (\text{F.23})$$

when  $f = 0$ . Note that since the Laplace equation is elliptic, this data does not determine  $f$  globally in our coordinate domain, but it is sufficient to determine it exponentially well near the UV boundary, and we only require  $f$  in the immediate vicinity of this boundary (i.e. we really only require its normal derivative) to define the asymptotic behavior of  $A, B, C, D$ . The behavior (F.18) will now ensure that the constraint  $\tilde{\alpha} = 0$  is satisfied. As mentioned above, the constant of proportionality,  $k$ , is unphysical and can be chosen arbitrarily.

### F.5. Summary

Our complete system, in either Euclidean or Lorentzian signature, is then the elliptic equations (F.2),(F.3),(F.4) and (F.12), together with their boundary conditions (F.9), (F.14) and (F.23). We see explicitly that, as indicated in section 8, the  $\mathbb{Z}_2$  symmetry (8.8) is manifest in the system. Furthermore, for fixed boundary locations, and once we have fixed the arbitrary scaling symmetry of the  $\tau, \theta$  and  $r_a$  coordinates (through the combined choices of  $c, k$  and the choice (F.14)), there is no further data to be specified. Whilst we have not rigorously demonstrated that this system is elliptic, this analysis strongly suggests that the solution is unique, having no additional parameters.

## Appendix G. Numerical Details

We define our coordinate domain using an auxiliary function  $h$ . We set  $h = 1$  on the lines  $x = 0$  and  $y = 0$ , and  $h = -0.6$  at  $x \geq 1, y = 1$  and  $y \geq 1, x = 1$ . We solve a Laplace equation for  $h$  in the interior of this region. Using this solution we then determine the coordinate position of the UV boundary at  $h = 0$  where we will demand  $f = 0$ , the IR boundaries at  $x = 0$  and  $y = 0$ , and hence the coordinate domain for our problem. Note this gives the required  $\mathbb{Z}_2$  symmetry of the UV boundary location, and for these choices, at large  $x$  the UV boundary tends to  $y = 5/8$ .

Furthermore we also determine an interior ‘boundary’ at  $h(x, y) = h_0$ , which satisfies  $0 < h_0^{d+1} \ll 1$  for computational purposes. To the IR of this interior boundary ( $h > h_0$ ) we use the metric variables  $A, B, C, D$  when solving the elliptic equations, and to the UV ( $h < h_0$ ) we use  $T, U, S, R$  which allows us to encode the correct UV behavior, without requiring large gradients that reduce accuracy and stability. The function  $f$  is now only defined in this UV region  $0 \leq h \leq h_0$ , where we must be able to translate between

$A, B, C, D$  and  $T, U, S, R$ . The initial guess for  $f$  is then taken to be  $h$ , and sensible initial guesses for the metric functions  $A, B, C, D$  and  $T, U, S, R$  are then made (using  $h$ ).

Due to the symmetry (8.8), we only implement the region  $y \leq x$  and use the symmetry to impose boundary conditions at  $x = y$ . In practice we truncate the asymptotic region at large  $x = L_{trunc}$  and simply require that normal gradients of all functions vanish there (i.e. Neumann boundary conditions). We also truncate the UV boundary to be at  $f = \epsilon$ , rather than  $f = 0$ , since the behavior of various terms in the elliptic equations are potentially rather singular there. We check that when the position of the large  $x, y$  boundaries is large compared to the bulk curvature length this truncation does not influence the solution. Similarly, when  $\epsilon$  is small, the difference between the solution for finite  $\epsilon$  and the extrapolated  $\epsilon = 0$  solution is also negligible.

The elliptic equations are second order finite differenced. The metric functions are relaxed using Gauss-Seidel iteration with the boundary conditions discussed earlier. Some under-relaxation is required depending on the resolution used. For some number of iterations  $f$  is not updated from its initial guess, to allow the metric components to settle to have sensible asymptotic behavior. Once this has occurred,  $f$  is also relaxed in the small UV region by the same method.

The value of  $f$  at the interior boundary  $h = h_0$  is required to solve  $R = kf^{d+1}$  there for some value of  $k$ . We solve this condition by updating  $f$  on this interior boundary by  $\delta f = \omega(R/kf^{d+1} - 1)$ , where  $\delta f$  is the update for  $f$  after each Gauss-Seidel step and  $\omega$  is a small number (say  $\sim 10^{-6}$  for the resolution used to produce the data shown here). This very slow update is required as the UV boundary is rather unstable numerically due to the singular nature of the elliptic equations there.

Ideally we only require the normal gradient behavior of  $f$  and thus really require only a tiny  $h_0$ , so the UV region where  $f$  is defined is very small. In practice, the singular behavior of the equations near the UV boundary mean  $h_0$  cannot be taken too small at a given resolution. However, we checked that for the values and resolutions used, the solutions were insensitive to the choice of  $h_0$ , provided it is small enough.

Results shown in the paper use the resolution  $320 \times 80$  in  $x, y$  (recall we only use the region  $y \leq x$ ) with  $L_{trunc} = 4$ ,  $\epsilon = 0.05$  and  $h_0 = 0.6$  for both  $d = 3, 4$ . The values of  $k$  were chosen for convenience to be 0.35 and 0.3 for  $d = 3, 4$  respectively.

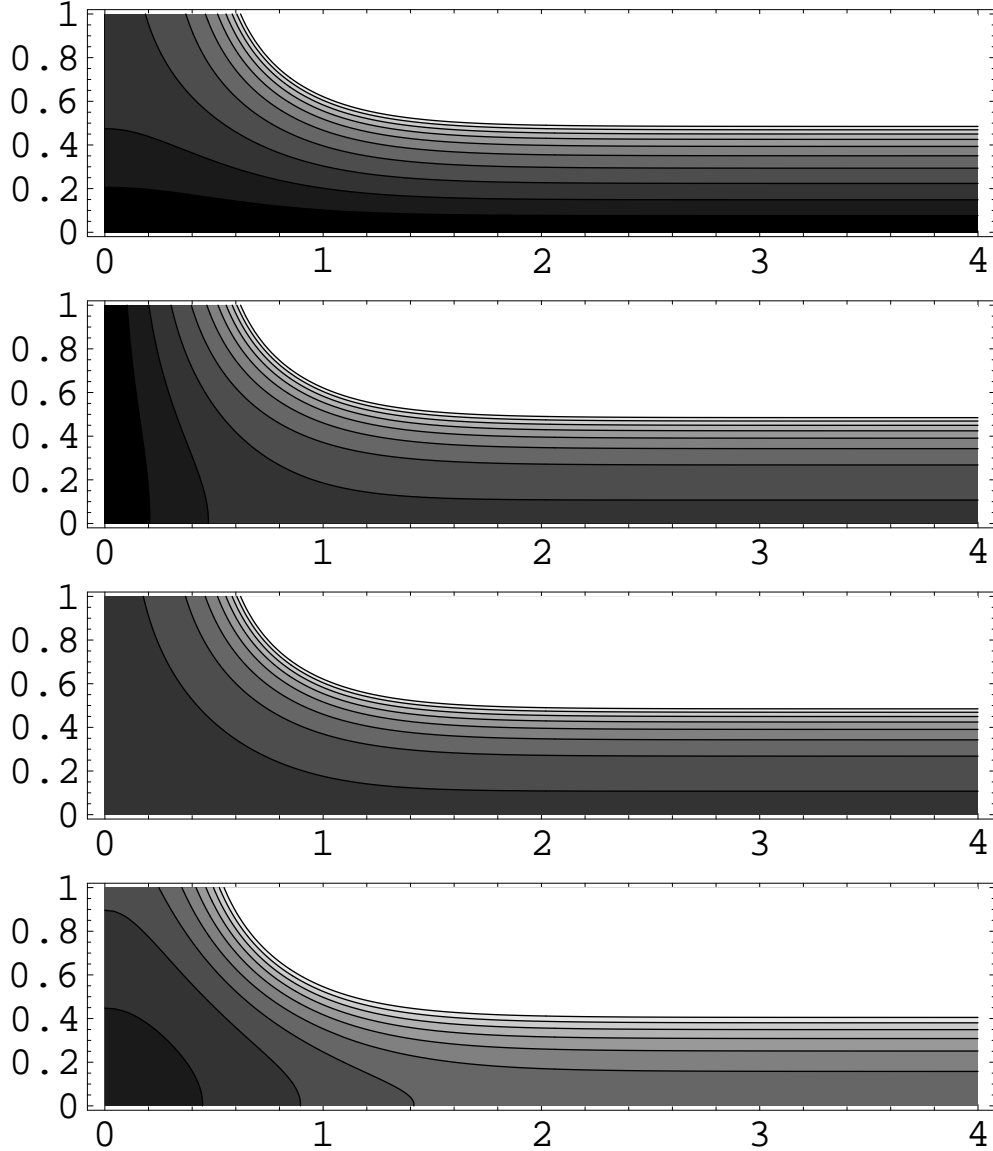


**Figure 12:** Contour plots of  $A, B, e^C, e^D$  in the  $x, y$  plane for  $d = 4$ .

We remind the reader that the explicit program code used to generate the solutions may be downloaded at <http://schwinger.harvard.edu/~wiseman/IRblackholes/>.

The procedure works very well, converging to a unique solution independent of initial guesses. We now give the results in more detail. The earlier figures 5 and 6 showed surface plots of the functions  $f$  and  $A, B, e^C, e^D$  for  $d = 4$ . In figure 12 we show contour plots of the functions  $A, B, e^C, e^D$  for  $d = 4$ . The functions appear qualitatively similar for  $d = 3$ , and can not be distinguished from these  $d = 4$  contour plots by eye.

Let us now check that the  $\tilde{\alpha} = 0$  constraint is correctly imposed in the UV. In figure 13 we plot, for  $d = 4$ , contours of  $R$  and  $f$  near the UV boundary, and indeed they agree

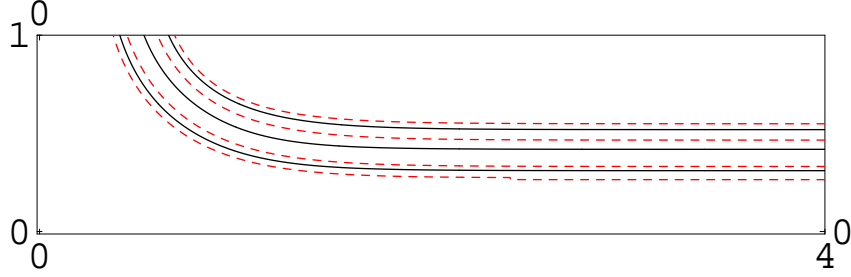


**Figure 13:** Plot showing contours of constant  $f$  (red, dashed) and  $R$  (black, solid) for  $d = 4$  near the UV boundary where  $f$  is defined. These are aligned, indicating that the constraint  $\tilde{\alpha} = 0$  is satisfied near the UV boundary.

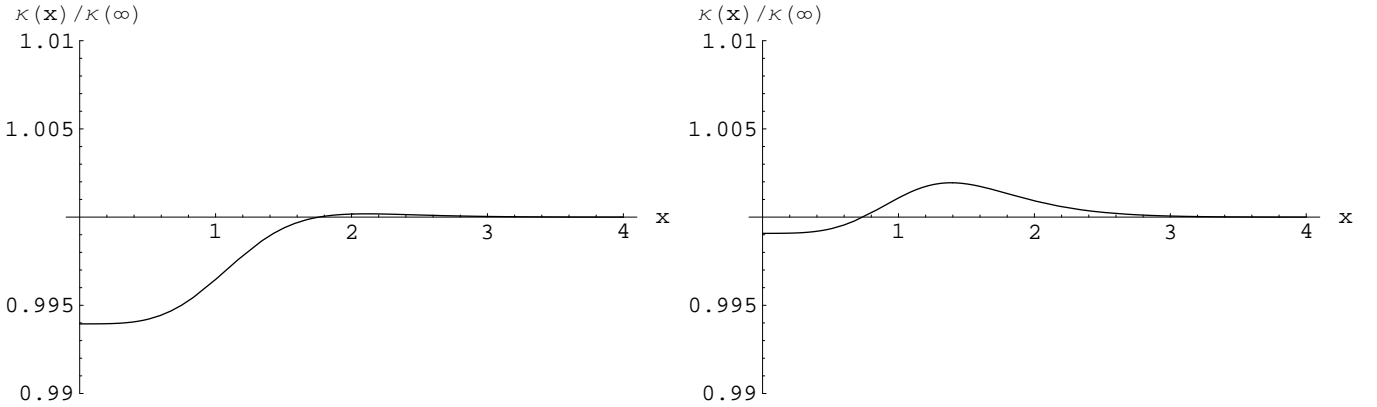


**Figure 14:** Plot showing violation of the  $\alpha = 0$  constraint in the IR. The proper gradient of the vanishing circle size,  $\kappa$ , is plotted against position on the boundary  $x$  for  $d = 3$  (left) and  $d = 4$  (right), normalized to its value as  $x \rightarrow \infty$ . The  $\alpha = 0$  constraint implies that this should be independent of  $x$ . Recall that we impose the constraints  $\beta = 0$  in the IR and  $\tilde{\alpha} = 0$  in the UV. Here we see that  $\alpha = 0$  is true to high accuracy in the IR, implying we have indeed solved the Cauchy-Riemann constraint system.

very well. One obtains a very similar plot for  $d = 3$ .

We directly impose the  $\beta = 0$  constraint in the IR and the  $\tilde{\alpha} = 0$  constraint in the UV. Thus we do not impose the  $\alpha = 0$  constraint in the IR and this gives a rather physical test of how well we solve the constraint system (F.6) by plotting the proper gradient of  $A$  at the IR boundary  $y = 0$ , i.e.  $\kappa(x) = e^{-D} \partial_y A|_{y=0}$ . We recall from (F.8) that the  $\alpha = 0$  constraint in the IR implies that  $\kappa(x)$  should in fact be a constant, and  $2\pi/\kappa$  gives the coordinate period of the two circles  $\beta, \tilde{\beta}$ . In figure 14 we plot  $\kappa(x)$  for the  $d = 3$  and  $d = 4$  solutions, and we see that they are both beautifully constant indeed, reflecting the fact that we have solved the Cauchy-Riemann constraint system to a high accuracy for the resolution used.



## References

- [1] G. 't Hooft, “A planar diagram theory for strong interactions,” Nucl. Phys. B **72**, 461 (1974).
- [2] S. B. Giddings, “High energy QCD scattering, the shape of gravity on an IR brane, and the Froissart bound,” Phys. Rev. D **67**, 126001 (2003) [arXiv:hep-th/0203004]; D. M. Eardley and S. B. Giddings, Phys. Rev. D **66**, 044011 (2002) [arXiv:gr-qc/0201034].
- [3] K. Kang and H. Nastase, “High energy QCD from Planckian scattering in AdS and the Froissart bound,” arXiv:hep-th/0410173; K. Kang and H. Nastase, “Heisenberg saturation of the Froissart bound from AdS-CFT,” arXiv:hep-th/0501038; H. Nastase, “The soft pomeron from AdS-CFT,” arXiv:hep-th/0501039; H. Nastase, “The RHIC fireball as a dual black hole,” arXiv:hep-th/0501068.
- [4] B. Lucini, M. Teper and U. Wenger, “The deconfinement transition in SU(N) gauge theories,” Phys. Lett. B **545**, 197 (2002) [arXiv:hep-lat/0206029]; B. Lucini, M. Teper and U. Wenger, “The high temperature phase transition in SU(N) gauge theories,” JHEP **0401**, 061 (2004) [arXiv:hep-lat/0307017]; B. Lucini, M. Teper and U. Wenger, “Properties of the deconfining phase transition in SU(N) gauge theories,” JHEP **0502**, 033 (2005) [arXiv:hep-lat/0502003].
- [5] O. Aharony, J. Marsano, S. Minwalla, K. Papadodimas and M. Van Raamsdonk, “A first order deconfinement transition in large N Yang-Mills theory on a small  $S^3$ ,” Phys. Rev. D **71**, 125018 (2005) [arXiv:hep-th/0502149].
- [6] R. D. Pisarski, “Finite Temperature QCD At Large N,” Phys. Rev. D **29**, 1222 (1984).
- [7] O. Aharony, J. Marsano, S. Minwalla, K. Papadodimas and M. Van Raamsdonk, “The Hagedorn / deconfinement phase transition in weakly coupled large N gauge theories,” Adv. Theor. Math. Phys. **8**, 603 (2004) [arXiv:hep-th/0310285].
- [8] E. Witten, “Anti-de Sitter space, thermal phase transition, and confinement in gauge theories,” Adv. Theor. Math. Phys. **2**, 505 (1998) [arXiv:hep-th/9803131].
- [9] I. R. Klebanov and M. J. Strassler, “Supergravity and a confining gauge theory: Duality cascades and  $\chi$ SB-resolution of naked singularities,” JHEP **0008**, 052 (2000) [arXiv:hep-th/0007191].
- [10] J. M. Maldacena and C. Nunez, “Towards the large N limit of pure N = 1 super Yang Mills,” Phys. Rev. Lett. **86**, 588 (2001) [arXiv:hep-th/0008001].
- [11] S. S. Gubser, C. P. Herzog and I. R. Klebanov, “Symmetry breaking and axionic strings in the warped deformed conifold,” JHEP **0409**, 036 (2004) [arXiv:hep-th/0405282].
- [12] J. Polchinski and M. J. Strassler, “The string dual of a confining four-dimensional gauge theory,” arXiv:hep-th/0003136.
- [13] S. Minwalla, ‘Black Holes in Gauge Theories’ (talks at the Post-Strings workshop at CERN, July 2004, and at the Tata Institute, September 2004.)

- [14] J. Polchinski and M. J. Strassler, “Deep inelastic scattering and gauge/string duality,” *JHEP* **0305**, 012 (2003) [arXiv:hep-th/0209211].
- [15] S. Hollands, A. Ishibashi and D. Marolf, “Counter-term charges generate bulk symmetries,” arXiv:hep-th/0503105.
- [16] I. Papadimitriou and K. Skenderis, “Thermodynamics of asymptotically locally AdS spacetimes,” arXiv:hep-th/0010138.
- [17] R. Gregory and R. Laflamme, “Black strings and p-branes are unstable,” *Phys. Rev. Lett.* **70**, 2837 (1993) [arXiv:hep-th/9301052].
- [18] R. Gregory and R. Laflamme, “The instability of charged black strings and p-branes,” *Nucl. Phys. B* **428**, 399 (1994) [arXiv:hep-th/9404071].
- [19] S. Gubser and I. Mitra, “Instability of charged black holes in anti-de Sitter space,” arXiv:hep-th/0009126.
- [20] R. Emparan and H. S. Reall, “A rotating black ring in five dimensions,” *Phys. Rev. Lett.* **88**, 101101 (2002) [arXiv:hep-th/0110260].
- [21] P. Creminelli, A. Nicolis and R. Rattazzi, “Holography and the electroweak phase transition,” *JHEP* **03**, 051 (2002) [arXiv:hep-th/0107141].
- [22] I. R. Klebanov and A. A. Tseytlin, “Gravity duals of supersymmetric  $SU(N) \times SU(N+M)$  gauge theories,” *Nucl. Phys. B* **578**, 123 (2000) [arXiv:hep-th/0002159].
- [23] W. Heisenberg, “Production of mesons as a shock wave problem,” *Zeit. Phys.* **133**, 65 (1952).
- [24] V. E. Hubeny and M. Rangamani, “Unstable horizons,” *JHEP* **0205**, 027 (2002) [arXiv:hep-th/0202189].
- [25] G. T. Horowitz and K. Maeda, “Fate of the black string instability,” *Phys. Rev. Lett.* **87**, 131301 (2001) [arXiv:hep-th/0105111].
- [26] O. Aharony, J. Marsano, S. Minwalla and T. Wiseman, “Black hole - black string phase transitions in thermal 1+1 dimensional supersymmetric Yang-Mills theory on a circle,” *Class. Quant. Grav.* **21**, 5169 (2004) [arXiv:hep-th/0406210].
- [27] S. B. Giddings and E. Katz, “Effective theories and black hole production in warped compactifications,” *J. Math. Phys.* **42**, 3082 (2001) [arXiv:hep-th/0009176].
- [28] G. T. Horowitz and R. C. Myers, “The AdS/CFT correspondence and a new positive energy conjecture for general relativity,” *Phys. Rev. D* **59**, 026005 (1999) [arXiv:hep-th/9808079].
- [29] S. Ferrara, A. Kehagias, H. Partouche and A. Zaffaroni, “AdS(6) interpretation of 5D superconformal field theories,” *Phys. Lett. B* **431**, 57 (1998) [arXiv:hep-th/9804006].
- [30] H. Weyl, “Zur Gravitationstheorie,” *Ann. Phys. (Leipzig)* **54**, 117 (1917).
- [31] R. Emparan and H. Reall, “Generalized Weyl solutions,” *Phys. Rev. D* **65**, 084025 (2002) [arXiv:hep-th/0110258].
- [32] C. Charmousis and R. Gregory, “Axisymmetric metrics in arbitrary dimensions,” *Class. Quant. Grav.* **21**, 527 (2004) [arXiv:gr-qc/0306069].

- [33] T. Wiseman, “Relativistic stars in Randall-Sundrum gravity,” *Phys. Rev. D* **65**, 124007 (2002) [arXiv:hep-th/0111057].
- [34] T. Wiseman, “Static axisymmetric vacuum solutions and non-uniform black strings,” *Class. Quant. Grav.* **20**, 1137 (2003) [arXiv:hep-th/0209051].
- [35] H. Kudoh, T. Tanaka and T. Nakamura, “Small localized black holes in braneworld: Formulation and numerical method,” *Phys. Rev. D* **68**, 024035 (2003) [arXiv:gr-qc/0301089].
- [36] B. Kleihaus and J. Kunz, “Static black hole solutions with axial symmetry,” *Phys. Rev. Lett.* **79**, 1595 (1997) [arXiv:gr-qc/9704060].
- [37] R. Emparan, G. T. Horowitz and R. C. Myers, “Exact description of black holes on branes,” *JHEP* **01**, 007 (2000) [arXiv:hep-th/9911043].
- [38] I. Zakout, “The C-metric black hole near the IR-brane in the AdS(4) space,” arXiv:hep-th/0210063.
- [39] J. F. Plebanski and M. Demianski, “Rotating, charged, and uniformly accelerating mass in general relativity,” *Annals Phys.* **98**, 98 (1976).
- [40] G. T. Horowitz and H. Ooguri, “Spectrum of large N gauge theory from supergravity,” *Phys. Rev. Lett.* **80**, 4116 (1998) [arXiv:hep-th/9802116].
- [41] L. Alvarez-Gaume, C. Gomez, H. Liu and S. Wadia, “Finite temperature effective action, AdS(5) black holes, and 1/N expansion,” *Phys. Rev. D* **71**, 124023 (2005) [arXiv:hep-th/0502227].
- [42] H. Schnitzer, “Confinement / deconfinement transition of large N gauge theories with N(f) fundamentals: N(f)/N finite,” *Nucl. Phys.* **B695**, 267 (2004) [arXiv:hep-th/0402219].
- [43] K. Rajagopal, “Mapping the QCD phase diagram,” *Nucl. Phys. A* **661**, 150 (1999) [arXiv:hep-ph/9908360].
- [44] M. G. Alford, K. Rajagopal and F. Wilczek, “QCD at finite baryon density: Nucleon droplets and color superconductivity,” *Phys. Lett. B* **422**, 247 (1998) [arXiv:hep-ph/9711395].
- [45] J. Berges and K. Rajagopal, “Color superconductivity and chiral symmetry restoration at nonzero baryon density and temperature,” *Nucl. Phys. B* **538**, 215 (1999) [arXiv:hep-ph/9804233].
- [46] M. Gyulassy and L. McLerran, “New forms of QCD matter discovered at RHIC,” *Nucl. Phys. A* **750**, 30 (2005) [arXiv:nucl-th/0405013].
- [47] T. Ludlam and L. McLerran, “What have we learned from the Relativistic Heavy Ion Collider?,” *Phys. Today* **56N10**, 48 (2003).
- [48] U. W. Heinz, “From SPS to RHIC: Breaking the barrier to the quark-gluon plasma,” *AIP Conf. Proc.* **602**, 281 (2001) [arXiv:hep-ph/0109006].

- [49] H. Heiselberg and A. D. Jackson, “Signatures of QCD matter at RHIC,” arXiv:nucl-th/9809013; H. Heiselberg and A. D. Jackson, “Anomalous multiplicity fluctuations from phase transitions in heavy ion collisions,” Phys. Rev. C **63**, 064904 (2001) [arXiv:nucl-th/0006021].
- [50] I. N. Mishustin, “Non-equilibrium phase transition in rapidly expanding QCD matter,” Phys. Rev. Lett. **82**, 4779 (1999) [arXiv:hep-ph/9811307].
- [51] L. Susskind, “Some speculations about black hole entropy in string theory,” arXiv:hep-th/9309145.
- [52] G. T. Horowitz and J. Polchinski, “A correspondence principle for black holes and strings,” Phys. Rev. D **55**, 6189 (1997) [arXiv:hep-th/9612146].
- [53] J. D. Brown and J. W. York, “Quasilocal energy and conserved charges derived from the gravitational action,” Phys. Rev. D **47**, 1407 (1993).
- [54] V. Balasubramanian and P. Kraus, “A stress tensor for anti-de Sitter gravity,” Commun. Math. Phys. **208**, 413 (1999) [arXiv:hep-th/9902121].
- [55] M. Henningson and K. Skenderis, “Holography and the Weyl anomaly,” Fortsch. Phys. **48**, 125 (2000) [arXiv:hep-th/9812032].
- [56] S. de Haro, S. Solodukhin and K. Skenderis, “Holographic reconstruction of spacetime and renormalization in the AdS/CFT correspondence,” Commun. Math. Phys. **217**, 595 (2001) [arXiv:hep-th/0002230].
- [57] K. Skenderis, “Asymptotically anti-de Sitter spacetimes and their stress energy tensor,” Int. J. Mod. Phys. A **16**, 740 (2001) [arXiv:hep-th/0010138].
- [58] P. Kraus, F. Larsen and R. Siebelink, “The gravitational action in asymptotically AdS and flat spacetimes,” Nucl. Phys. B **563**, 259 (1999) [arXiv:hep-th/9906127].
- [59] C. Fefferman and C.R. Graham, “Conformal invariants,” in *Elie Cartan et les Mathematiques d’Aujourd’hui*, Asterisque (1985) 95.
- [60] M. Henningson and K. Skenderis, “The holographic Weyl anomaly,” JHEP **9807**, 023 (1998) [arXiv:hep-th/9806087].